Kaunas University of Technology

Faculty of Electrical and Electronics Engineering

Investigation and Development of Energy Harvesting Devices for Supplying Low Power Sensors

Master's Final Degree Project

Chandana Ravikumar

Project author

Prof.Vytautas Markevicius

Supervisor

Kaunas, 2020

Kaunas University of Technology

Faculty of Electrical and Electronics Engineering

Investigation and Development of Energy Harvesting Devices for Supplying Low Power Sensors

Master's Final Degree Project

Electronics Engineering (6211EX012)

Chandana Ravikumar

Project author

Prof. Vytautas Markevicius

Supervisor

Dr. Ramunas Ramanauskas

Reviewer

Kaunas, 2020

Kaunas University of Technology

Faculty of Electrical and Electronic Engineering

Chandana Ravikumar

Investigation and Development of Energy Harvesting Devices for Supplying Low Power Sensors

Declaration of Academic Integrity

I confirm that the final project of mine, Chandana Ravikumar, on the topic „Investigation and development of energy harvesting devices for supplying low power sensors " is written completely by myself; all the provided data and research results are correct and have been obtained honestly. None of the parts of this thesis have been plagiarised from any printed, Internet-based or otherwise recorded sources. All direct and indirect quotations from external resources are indicated in the list of references. No monetary funds (unless required by Law) have been paid to anyone for any contribution to this project.

I fully and completely understand that any discovery of any manifestations/case/facts of dishonesty inevitably results in me incurring a penalty according to the procedure(s) effective at Kaunas University of Technology.

Chandana Ravikumar _____

(name and surname filled in by hand)

_____

(signature)

Ravikumar Chandana. Investigation and development of energy harvesting devices for low power sensors. Master's Final Degree Project / Prof. Vytautas Markevicius; Faculty of Electrical and Electronic Engineering, Kaunas University of Technology.

Study field and area (study field group): Electronics Engineering, Engineering Science.

Keywords: multilayer piezoelectric vibration energy harvester;PVDF;optimization proofmass gap; rayleigh damping;temperature dependence.

Kaunas, 2020. 67p

Summary

Wireless sensor networks conventionally depend on rechargeable batteries for power supply where energy is always brought to the device externally causing high maintenance efforts. There is a need for shift in paradigm. Powering devices need to be done differently by using energy that is already available in the device location, consequently enter the domain of energy harvesting systems. This thesis proposes an alternative solution to supply an entire system by converting ambient vibrations into electricity using piezoelectric effect. The motive is to present the findings that have led to the fabrication and development of multilayer PVDF energy harvester having power density of 20.23 $mW/cm^3/g$, generating at least 14 V_{RMS} voltage and 435 μW power for optimal load impedance of 460kΩ being subjected to an acceleration of 0.4g.

The study explores parameters including gap and proof mass, that can affect the damping of cantilever to optimize the design of energy harvester. A finite analysis is conducted using Rayleigh damping coefficients in COMSOL Multiphysics software. Outcome of modelling and testing has resulted in the best possible optimization for the energy harvester. Relationship between actuator input and output parameters is established. Temperature dependence of energy harvester on load rms voltage, resonance frequency, internal resistance and actuator acceleration is analyzed. Comparing with the smallest gap and proof mass, simple engineering approach for the optimization of PVEH has resulted in increasing the output up to 5 times.

Ravikumar Chandana. Magistro baigiamasis projektas / vadovas Prof. Vytautas Markevicius ; Kauno technologijos universitetas, Elektros ir elektronikos fakultetas.

Studijų kryptis ir sritis (studijų krypčių grupė): Elektronikos inžinerija, inžinerijos mokslai.

Reikšminiai žodžiai:daugiasluoksnis pjezoelektrinis vibracijų energijos kaupiklis; PVDF; masės tvirtinimo tarpo optimizacija; Rėlėjaus slopinimas; temperatūros priklausomybė

Kaunas, 2020. 67p.

Santrauka

Belaidžiai jutiklių tinklai paprastai priklauso nuo įkraunamų baterijų, kurioms reikia daug priežiūros, nes energija į prietaisą patenka iš išorės. Todėl yra poreikis esminiams pokyčiams, maitinimo prietaisai turi būti daromi kitaip, naudojant energiją, kuri jau yra įrenginio vietoje, pasinaudojant energijos rinkimo teikiamomis galimybėmis. Šis magistro darbas siūlo alternatyvų sprendimą, kaip aprūpinti visą sistemą energija, paverčiant aplinkos vibraciją elektros energija pjezoelektrinio efekto dėka. Šio tyrimo tikslas yra sukurti daugiasluoksnį PVDF energijos rinktuvą, kurio galios tankis yra 20.23 $mW/cm^3/g$ ir sukuriantis mažiausiai 14 V_{RMS} įtampą ir 435 μW galią 0,4 g pagreičiui prie optimalios 460kΩ apkrovos.

Šiame tyrime tiriami parametrai, įskaitant tarpą ir apkrovos masę, kurie gali turėti įtakos gembės slopinimui, kad būtų galima optimizuoti energijos rinktuvo dizainą. Išsami analizė atliekama naudojant COMSOL Multiphysics programinę įrangą. Remiantis modeliavimo ir bandymų rezultatais, buvo nustatytos geriausios įmanomos šio energijos generatoriaus darbo sąlygos. Nustatytas ryšys tarp pavaros įėjimo ir išėjimo parametrų. Nagrinėjama energinio rinktuvo temperatūros priklausomybė nuo rms įtampos, rezonanso dažnio, vidinio pasipriešinimo ir pavaros pagreičio. Palyginus su pradiniais, kitų gamintojų bandiniais, pritaikius vibracijų energijos surinkimo sistemų (PVEH) optimizavimą, išgaunama galia padidėjo 5 kartus.

Acknowledgement

Firstly I am truely grateful for all the blessings God has bestowed upon me and heart fully thank my mother Mrs Nalini Tumkur Shivaprakash and my father Mr Ravikumar Halehalli Chikkanna for their love and support throughout my college career.

I thank my advisor Prof. Vytautus Markevicius, for his kindness and guidance throughout the study in Kaunas University of Technology. I extend my thanks to Mr Donat Ponamariov founder of UAB Nanoenergija‘ for supporting this research and also thank Prof. Dangirutis Navikas, Prof. Darius Andriukaitis, Dr Mindaugas Cepenas, lecturer Neringa Dubauskiene and Mrs Olusola Abayomi for their valuable advice.

I also thank my colleagues in Interactive electronic systems laboratory for their help throughout my research and wish them all the best in their future endeavors.

Table of contents

List of abbreviations and terms

Abbreviations

PVEH– Piezoelectric vibration energy harvester;
PE- Piezoelectric;
PVDF - Polyvinylidene fluoride;
VEH-Vibration energy harvester;
PEC-Piezoelectric cantilever;
IoT- Internet of things ;
PEH- Piezoelectric energy harvester ;
FUC- Frequency up-conversion;
PE- Piezo electric ;
MEMS- Microelectromechanical systems;
IDE-Interdigital electrodes;
AI-Artificial intelligence;
MPPT-Maximum power point tracking;
ZnO- ZincOxide nanoparticles;
BPFs-Block pulse functions;
MDOF-Multi direction of freedom;
PMN-PT - Lead magnesium niobate-lead titanate – piezocrystal;
PZT - Lead zirconate titanate – piezoceramic material;
KNN-Sodium potassium niobate;
AlN-Aluminium Nitrate;
SSHI-Synchronized switch harvesting on inductor;
ICP-Integrated circuit piezoelectric accelerometer;
SSPB- Single supply pre-biasing;

Terms

V_{RMS} -Root Mean Square voltage generated by PVEH;
R_i-Internal ressistcne ;
V_{CV}-Coil excitation voltage suppied to actuator ;
V_{AV}-Acceleration voltage measured by analog accelerometer ;
Acc-Actual acceleration measured by digital accelerometer;
$Coeff_{AV}$-Coefficient of analog accelerometer voltage ;
$A_{Coeff_{AV}}$-Acceleration calculated using $Coeff_{AV}$;
$Coeff_{CV}$- Coefficient of coil excitation voltage ;
$A_{Coeff_{AV}}$-Acceleration calculated using $Coeff_{CV}$;

List of figures

List of tables

Introduction

Research Relevance, Aim and Objectives

Progress comes from giving meaning to technology. Embodying this approach, thesis work showcases a focused activity aimed at identifying methods, techniques and directions for devices and systems sustainable with regard to energy. Energy harvesting is revolutionizing the way to power devices allowing to build end-to-end IoTs cases. A lot of elements are getting integrated into a single chip that is able to serve a diverse set of purpose. Hence with more and more devices getting integrated it has become compelling than ever before to rely on energy harvesting systems. Energy harvesting technology is an innovation that enables other innovations meaning that people resort to energy harvesting to power other application which may or may not have existed otherwise. This research work presents an energy harvesting system by leveraging the open power of vibration.

Object of this research - multilayer PVEH(peizoelectric vibration energy harvester)– consists of relatively flexible cantilever beam covered with PVDF, which is in turn enveloped with electrodes enabling to collect charge developed across deformed PE material. This cantilever beam will impact on a rigid mechanical support (steel substrate), which is incorporated to harvester with the aim to widen its operational frequency range and prolong lifetime. The power output of a particular PVEH depends upon many internal and external factors like internal resistance and ambient temperature respectively. Study of the influence of such factors is crucial as the energy in ambient vibrations is inherently low. Presently, low output performance along with small bandwidth is still the most challenging issue before practical deployment of PVEH [1]. Addressing such difficulties this research develops a real energy harvester that has power density of 20. 23 $\mathrm{mW/cm^3}$ /g, generates at least $14V_{RMS}$ voltage and 435 µW power for 0.4g acceleration. This result is compared with other published works in chapter 8 and the result is well justified by the extent of optimization, investigation and analysis shown in the following chapters.

The aim of this thesis is to develop an optimized energy harvesting system that can be applied to real world problems by producing an efficient energy harvesting solution focused on scavenging vibration energy from ambient sources abundant in both natural and industrial environments. To achieve this goal, the following tasks are set:

1. Perform literature analyses of the research ongoing in the field of energy harvesting, largely focusing on piezoelectric energy harvesters and recognize exiting problems and performance enhancement techniques;
2. Formulate equations to calculate internal resistance and power generated using experiment data;
3. Calibrate the actuator used with respect to the input supply frequency, input coil excitation voltage (V_{CV}) and acceleration voltage (V_{AV});
4. Design and perform an analytical, theoretical and practical investigation with a measurement error of less than ± 5% on commercial PE cantilevers that can help in designing and optimizing of proposed PVEH;
5. Develop an accurate finite element model of proposed PVEH, which would allow investigation of harvester dynamic and electric response;

6. Propose a fabrication method to work with multilayer PVDF material and steel substrate for the construction of PVEH samples so that at least 1mW power is achievable per unit acceleration provided;
7. Perform comparitive study of the results of the proposed enhanced PVEH prototype with its counterparts from published sources;
8. Practical evaluation of temperature stability of PVEH, in the range of [-30 ℃; 60 ℃];

Mismatch between ambient vibrations and system resonant frequencies may occur in harvesters due to un-constant nature of excitation frequency, environment temperature fluctuation, manufacturing tolerances and other reasons[1], hence an important step was taken to test the proposed harvester against varying temperatures. As it is already stated above, one of the objectives is to review and summarize recent publications related to the field of energy harvesting. Vibration energy conversion principles are briefly explained, summarizing their basic operation principles and a deeper understanding is given about piezoelectric conversion. Only piezoelectric transduction mechanism (as well as the main properties of PE materials) is described and analyzed more in detail, since objects of this research are operating on the basis of this conversion principle. Earliest configurations of vibration energy harvesters focused on simple oscillators aiming to exploit resonance phenomenon under harmonic excitation. However, recent research has been directed towards more sophisticated energy harvester configurations that could as well harvest energy from random ambient vibrations. As a result, a part of recent research in focused on nonlinear and complex scavenging systems. In comparision to their liner counterparts, non-linear energy harvesters demonstrate better performance under broadband excitation as well as longer device operation lifetime[1]-[3]. Not only typical PE energy harvester designs but also recent non-linear design implementations are discussed in the first chapter.

Vibration energy harvesting(VEH) using multilayer piezoelectric cantileverd(PECs) as in most of the published works are complicated to be implemented in large scale applications. In order to design a wide frequency bandwidth piezoelectric vibration energy harvester (PVEH) for a specific application, one normally has to rely on commercially available PEC(piezoelectric cantilever) beams. But these commercially available PECs not readily available off the shelf with any geometry and with required characteristics. Hence an engineer has to come up with a customised design of PVEH that can fullfill the purpose of the device application. In the process of designing of a PVEH specific analytical or numerical model needs to be established to estimate the output power of the system. A study on these models is given in [2],[3]. This research work depends on finite analysis conducted using COMSOL Multiphysics software. In this type of simulation, loss factor is commonly used, but it produces a model that does not fit experimental data well. In order to build a true model, Rayleigh damping coefficients are measured to use in simulation. This results in a closer fit of modeling and experimental data and a 5 times better output voltage of optimized PVEH comparing with using the smallest gap and mass will be discussed in chapter 6. Tipmass refers to the proof mass fixed to the free end of the cantilever and gap is the distance between tipmass and the fixed end of the cantilever

Document structure

The thesis is divided into eight sections. Research development pathway presented below gives the sequence of actions taken to meet the research objectives and achieve the final aim of study.

- Chapter 1 is a comprehensive literature review that recognizes the problems in energy harvesting, presents main topics related to the concept of the energy harvesting, reviews recent and most relevant literature and discussion on studies performed in this area. Review on different methods employed to convert vibration energy into electricity is presented with particular emphasis on PE transduction. The latter is followed by broad review of PEH configurations, types of harvesters, shapes, PE materials, importance of poling direction, interfacing circuits, application of energy harvesting, highlighting main issues dealt with the most popular harvester designs along with some performance enhancement techniques.
- Chapter 2 is dedicated to the theoretical calculations involved in piezo-based power harvesting systems, including properties and governing equations. Circuits, structural diagrams and operating conditions of the transducer are presented. Theoretical analysis, estimation of power and energy is done, internal resistance calculations and theoretical measurement accuracy is evaluated.
- Chapter 3 presents a study on calibration of the excitation device-actuator used in experiments. Since acceleration produced by actuator is not same for all input frequencies, acceleration becomes a function of input supply frequency, this relation is extended to V_{CV} (coil excitation voltage suppied to actuator) and V_{AV}(acceleration voltage measured by analog accelerometer).
- Chapter 4 introduces the initial considerations in experiment process, commercial PE cantilevers are tested, internal resistance, power, energy is calculated and rectifier circuit for AC-DC conversion is discussed.
- Chapter 5 describes the experimental procedures conducted on commercial cantilevers. In this section, the characteristics, optimization of tipmass(proof mass), gap and cantilever size is done from the perspective of performance enhancement.
- Chapter 6 introduces the developed finite element model of proposed PVEH and describes all theoretical and practical investigation performed during the research period involving a number of different PE energy harvester configurations - varying harvester's dimensions and shape, PVDF material of different manufacturers, pattern of PE layer segmentation, parameters of the connected electric circuit, and rigid support thickness - finally introducing an enhanced design of PVEH. It also explains the fabrication process of proposed harevster and challenges involved.
- Chapter 7 presents the temperature dependence measurements where tests are performed in a temperature test chamber in the range of -30℃ to 60℃. All output results described in the temperature effect section were investigated in the mentioned chamber. Effect of temperature on resonant frequency, coil excitation voltage and load rms voltage of proposed harvester is depicted and compared with the temperature dependence of commercial cantilevers.
- Chapter 8 is devoted to the comparitive study of the proposed enhanced PVEH prototype with its counterparts from published works. Working of different types of PE harvesters with regard to power output, input provided and area power density is compared and discussion on key problems and suggestions for future research and development is presented.

1. Literature review

1.1. Significance of piezoelectric vibration energy harvesters

Today the world is about‘ Enabling the Internet of Things’which is noting but making things smarter. Smart watch, smart building, smart city, smart health, smart agriculture, intelligent transportation, industry, security, marine and so on. For a smart home or a smart city to be smart, the process is the same as it is for a human being. For one to be smart information is required. One can feel, hear, smell, see things and this data is transmitted to our brain which essentially makes sense of it helping us to act, open our mouth to hopefully say something smart. Likewise, the process is the same for a smart city. The sensing devices generate data, algorithms in the cloud decode it, meanwhile the traffic lights turn from red to green, air conditioning goes on or off and so on. However, after a long day of work one can go home and rest to wake up the next day fully recharged. Perhaps this is precisely what the IoTs cannot do. When the IoTs is exhausted, it dies. Billions of distributor sensors are spread out in an enormous area and powering them becomes the obvious challenge. Conventionally there are two ways of supplying power. Firstly with the use batteries. The batteries themselves are not very expensive but sending a person to swap out thousands of batteries is expensive or rather impossible because in many locations it is mostly not feasible to do maintenance. Another option is use of plug-in cables which is impractical and moreover quite unpleasant for an end user to charge the device frequently. So by far powering seems to be a fundamental problem for launching high volume IoTs solutions. In cold countries temperature sensors are embedded in the road for a simple application that is when the roads get cold it becomes slippery and icy so salt needs to be thrown on the roads. A sensor could be placed in a road 5 years ago but then somebody had to go back and swap a battery now and then. It seems to be an unrealistic application when a highway needs to be closed down because the sensors ran out of battery power. When a sensor is installed in a road it should necessarily outlast the road because the alternative is not a practical option. The whole application will not work because the cost of maintenance and ownership of the system far exceeds the installation cost. Either the problem of swapping the batteries needs to be fixed or the whole idea is dropped. This becomes a game changer for many electronic applications.

There is a need for shift in paradigm. Traditionally, energy is always brought to the device, whether it is through a cable or a battery. But now it needs to be done differently by using energy that is already available in the device location entering into the domain of energy harvesting. After a device is purchased it is brought out of the box and is plugged in for power supply, then it works. However, for IoTs there is need to think a few steps further. We should get past the old ‘plug and play‘ system of using the device and move to‘ plug and forget‘. Here ‘forget’ is defined as outlasting the application that the device is meant for. For example if a sensor is being embedded in a road it should essentially outlast the road. On these lines the solution would be to install PVEH under the road to extract energy from the movement of vehicles and use it to power the temperature sensor installed in the road.

1.2. Challenges in energy harvesting

WSNs are predicted to cover a huge portion of IoTs systems. On the whole, engineers look for energy-neutrality, which is nothing but harvesting as much energy as possible and converting with high efficiency to maximize the quantity of useful work done[4],[5] however this presents complicated optimization problems for system designers which are discussed in this section.

Energy harvesting has applications like the climate management projects where in a new office building thousands of sensors are installed where when one walks into a room and the lights turn on or the air conditioning gets optimized based on the flow of people through the building. This is a typical example where PE sensors and PE energy harvesters are applied. Another exciting application of energy harvesting is smart watches. The Swiss watch manufacturers are about to launch a smart watch that is able to perform step counting with integrated accelerometer that can receive notifications from phone [6], such watches conventionally had to be charged frequently which caused an unpleasant user experience so the average Fitbit could end up somewhere in a drawer not being used within 6 months since day of purchase. Hence, the challenge was to make this hydrid watch to have the same user experience as that of a normal watch but with added features. Recent advancements have made this possible. Behind the dial of the watch there is a small solar panel and it is completely invisible so the dial blocks pretty much all of the light except for about 10% of light which is able to pass through the dial and reach the solar panel. This small amount of power extracted is sent to the chip which powers the entire system. Likewise there are many game changing innovations in medical applications, wearables, smart logistics, Industrial IoT, asset tracking and so on that are enabled by energy harvesting technologies.

Energy harvesting could be done from radio frequency signals in some cases even GSM or wi-fi signals contain trivial amount of energy, temperature differences like our skin and outside temperature or machine generating heat, piezoelectric like vibration movements or even delicate movement of human beating heart. There is energy present all around us that can be used in powering devices. Energy harvesting is perhaps one of the oldest ideas which is ironically still present today as it has not yet seen large scale commercial applications. The reason is because of few historical problems in 'ambient' energy harvesting discussed below.

- **Low energy output**

The obstacle of low energy output is quite obvious. The amount of energy that can be obtained from the sources around is certainly very low in μW range. Hence it is mostly unlikely to have mobile phones or laptops being powered by harvesting energy. However in the last few decades efficiency of devices have gone up enormously which means the amount of energy needed to perform certain functions in an electronic device has dropped dramatically. For instance, mobile phones are charged almost every day, the moment an efficiency gain is reached there is a tendency to add more features to the product so the consumption is roughly the same. Better efficiency, more features and same consumption. However in the case of IoTs the scenario is slightly different where the efficiency is improved enormously with low power sensing, computing and also the features are almost the same. Since the features have remained the same, the efficiency has become better and the consumption has reduced[4],[6]. Therefore, for the first time in history it has become feasible to actually use this little bit of energy that is around us to power devices. Hence the first challenge of utilizing small amount of power is solved by the energy technology development.

- **Low voltage output**

From trivial sources very low voltages maybe as low as 40mV to 100mV is extracted. This small voltage will not suffice because usually devices operate out of 3.6 V or higher. Although the voltage is boosted from 40mV to a higher voltage, it is usually a tedious task. Researchers can now do it over

92% efficiency starting as low as 40mV using A I powered MPPT (Artificial intelligence powered maximum power point tracking) [5],[6]

- **High amount of external components**

Large number of external components results in high form factor. The footprint on the PCB becomes too big and it becomes no longer suitable for the application in the sense that it will be unable to fit in a watch or a very small tracking device [6]. Hence using external components as less as possible is recommended.

- **Large form factor on PCB**

The design challenge that presents itself in a typical power transfer circuit of an energy harvesting system is to make sure that the combination of harvester and input converter can amplify harvested energy. In other words, the aim is to have least conversion losses and hence to design the converter according to vouch for maximum power transfer by impedance matching possibly with the help of MPPT. Hence it is crucial to build a mm^2 system that can help meet the design challenges to achieve energy-neutrality [5]. Some recent advances in processing electronics are presented in [6]-[8].

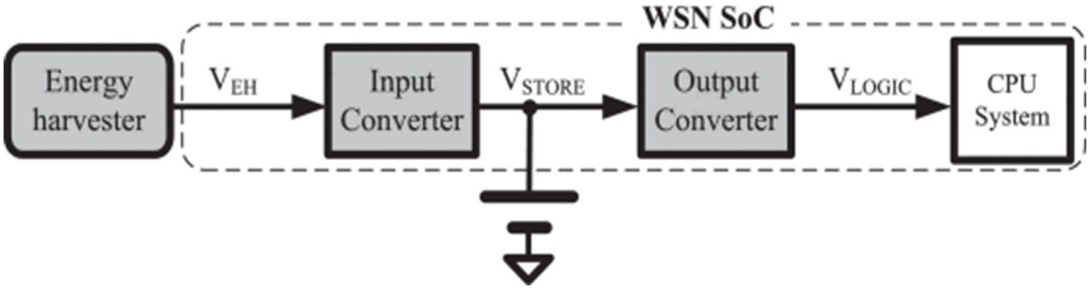

Fig 1. Flow chart of power conversion in an energy harvesting device[5]

The main constraint of the standard circuit is that a large portion of charge generated by the transducer is used to charge up its own internal capacitor leaving only a small portion to be delivered to the external capacitor. This loss in charge reduces the amount of electrical energy that can be harnessed and hence reduces the rectifying efficiency of the standard circuit. A better option to further boost the rectifying efficiency is a non-linear circuit which could extract charge synchronously. The charge generated is extracted whenever the piezoelectric voltage reaches the maximum point or minimum point. It is not always possible to adjust the circuit impedance with the optimum load required when standard bridge rectifier circuit is used. Hence, a buck and boost DC-to-DC converter could be a viable option which converts and regulates voltage essential to provide output voltage to the energy storage device so that optimum impedance to the transducer is guaranteed and indifferent towards the connected load [5]-[9]. Leteuver et al. claimed that an 84 % high efficiency and maximum harvester power of 1.5 mW was achieved by buck-boost converter that can trace the acceleration and vibration frequency dependence of harvesting device [10]. Lallart and Guyomar [11] developed a Synchronized Switch Harvesting on Inductor (SSHI) having an efficiency of 160 % over standard rectifier. Electrical energy is generated when the external force is damped by the PE transducers. However, because of the internal shunt capacitance, the transducer using with a resistive load usually does not provide sufficient damping force [12]. Dicken et al., demonstarated that it is pluasible to improve the damping force of the PE transducers by a circuit they designed, a dedicated circuit that is able to

synchronously discharge the generated charge to the load at the maximum or minimum point of each cycle and immediately followed by a pre-charge step. With the assumption that the charge oscillation is in phase with the vibration of the PEC, Fig. 2 illustrates the system. Precharging causes the PEC to bend having a larger amplitude and hence larger output voltage. By adopting the pre-biasing circuit efficiency of the PE transducer could be increased by at least 2 times and at most 10 times[13].

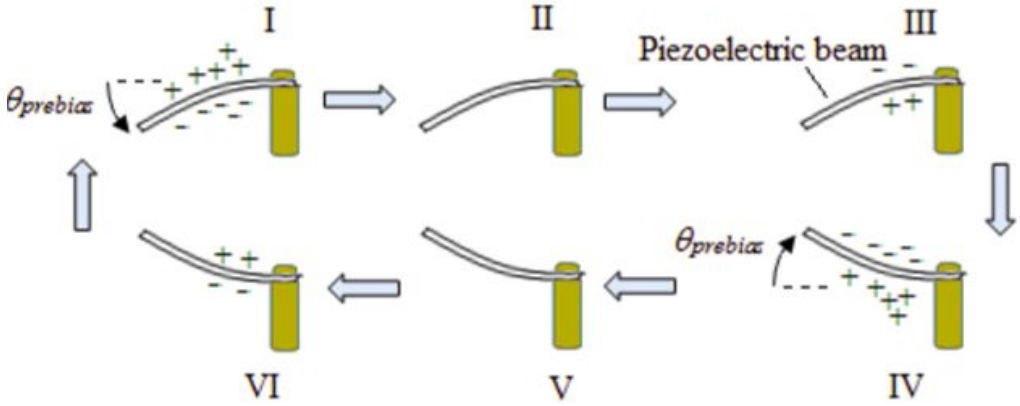

Fig 2. The movements of cantilever and charges corresponding to the processes I - VI [13].

1.3. Types of Vibration energy harvesting

Random displacements, including human activities from running, heartbeat, to respiration, mechanical vibrations from industrial machinery and transport vehicle etc are all ambient kinetic sources. Harvesting kinetic energy based on PE materials can be categorised into “fluid, ” “strain ” and “vibration” [14] Fluid energy harvesting uses fluid flows from wind, water, ocean,etc. Strain energy harvesting devices are associated with relative distortion and variation of the mechanical sources like compression of roadway vehicle, extension of muscle and so on. On the other hand the principle on which strain energy harvesting works is without inertial force or resonance vibration. A simple configuration of spring-mass-damping system is the working principle of vibration energy harvesting (VEH). Vibration amplitude and excitation frequency is taken into account in VEHs. There will be a drastic drop in power generation if there is any fluctuation in the excitation frequency away from the resonance. Widening the device frequecny bandwidth before practical installation is challenging therefore non linear VEHs are preferrred to linear counterparts in this case.

Electromagnetic, electrostatic and piezoelectric are the main transduction mechanisms.Also, triboelectric is an imminent energy harvesting concept in the recent few years[15]. The use of permanent magnets in electromagnetic energy harvesters produces power from induced current in magnetic fields but it occupies more space which makes it mechanically compelx. Whereas, higher energy conversion capacity at low frequencies is seen in piezoelectric harvesters as compared to electromagnetic harvesters for devices smaller than $1cm^3$ and hence for low operating (below 100 Hz) PEHs are most suitable. Electrostatic energy harvester works on sudden static electricity which is hard to secure and is left with only a few applications due to its low current. PVEH provide the needed voltage immediatley not requiring a separate voltage source as needed in electrostatic conversion. On the whole, although each of the above mentioned principles can produce significant quantity of energy. Easy architectures, higher energy density and immanent reciprocal conversion capability are all the advantages of PVEHs which make it more attractive along with the added feature of ease of scaling of piezoelectric material in micro and nanoscale devices [14]-[16].

1.4. Types of Piezoelectric materials

The first naturally occurring piezoelectric material is quartz, french physicists Jacques and Pierre Curie discovered it in the year 1880. Many natural and synthesized piezoelectric materials are found within the last 140 years that show remarkable properties to accomodate various applications. They are grouped in the following manner.

- **Inorganic piezoelectric material**

Inorganic PE matter is largely applied to mechanical energy harvesting and is grouped into firstly PE crystals comprising of a single crystal structure and are naturally piezoelectric eg like quartz film, and secondly piezoelectric ceramics like lead zirconate titanate $Pb[Zr_xTi_{1-x}]o_3$ with $0 \leq x \leq 1$ and barium titanate ($BaTiO_3$). Soon as poling is over, piezoelectric ceramics comprising of numerous tiny crystals with random crystal orientations start showing piezoelectricity.

- **Bio-Piezoeletric material**

Piezoelectric traces are found in biological tissues such as silk, bone and also in microbes and specific viruses. Swim bladder of CatlaCatla fish is an efficient bio-piezoelectric nanogenerator, having a big piezoelectric coefficient (d_{33} of ~22 pC/N), produces 10V of open-circuit voltage and 51nA of short-circuit current and ~4 W/cm^2 of peak output power when the organ is pressed by human finger or when a perpendicular compressive force (~1.4MPa) is applied [17]. The bio-piezoelectric materials can possibly show an environment friendly approach to energy generation provided biotechnology techniques facilitates big scale production and simple biodegradation. One of the drawbacks of bio-piezoelectric materials is small life span and non reuseability.

- **Piezoelectric polymers**

PE polymers such as PVDF and its copolymer poly(vinylidenefluoride-co-tri-fluoroethylene) (P(VDF-TrFE)) in comparison to inorganic PE materials are inherently flexible, easy for processing and mechanically strong making them desirable for flexible energy harvesting scenarios. The PE material used in this research is PVDF which is semi crystalline solid in homogenous structure. Manufacturing of the polymer is similar to that of peizoelectric ceramics usually by undergoing the poling process which is explained in the next sub section. PVDF exists as five polymorphs namely $\alpha, \beta, \gamma, \delta$, and ε. However, researchers have found that only β -phase PVDF shows strong piezoelectricity [18],[19].

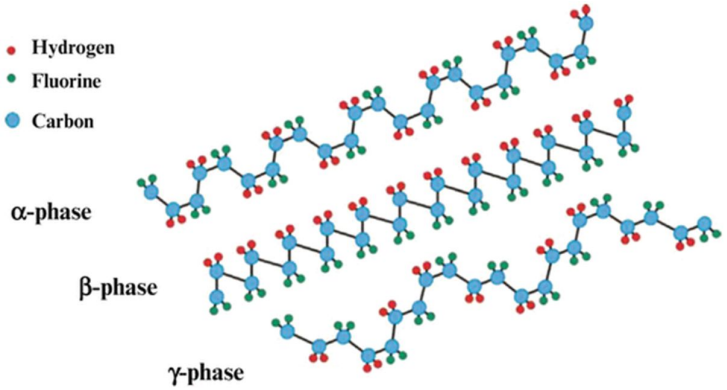

Fig 3. Atomic structure of PVDF adopted from [18]

- **Heterostructural materials**

Materials made of PE ceramics and polymers have great potential for energy harvesting as they acquire prominent PE properties of ceramics and the mechanical properties of polymer. For example, the PE polymer composites ($PZT-PVDF, BaTiO_3-PVDF$) show high flexibility,dielectric permittivity and breakdown strength thats get the better of more than one PE material. $FaPbBr_3$ nanoparticles and PVDF polymer combine to form a heterostructural material $FaPbBr_3-PVDF$, a PE composite nanogenerator that can generate voltage and current of 29.5 V and 6.2 $\mu A/cm^2$respectively[20].

1.5. Fundamentals of Piezoelectricity

Hankel came up the term 'piezoelectricity' which comes from the Greek word for 'press'. The word piezoelectric means that electric charge is created when mechanical stress is applied upon the PE material. Nevertheless, the process is reversed when electric field is applied resulting in changing the shape of the material, this is known as converse/reverse piezoelectric effect (Fig 4). Lippmann estimated this and Curie later confimed that the converse effect held true in 1881 [21],[22].

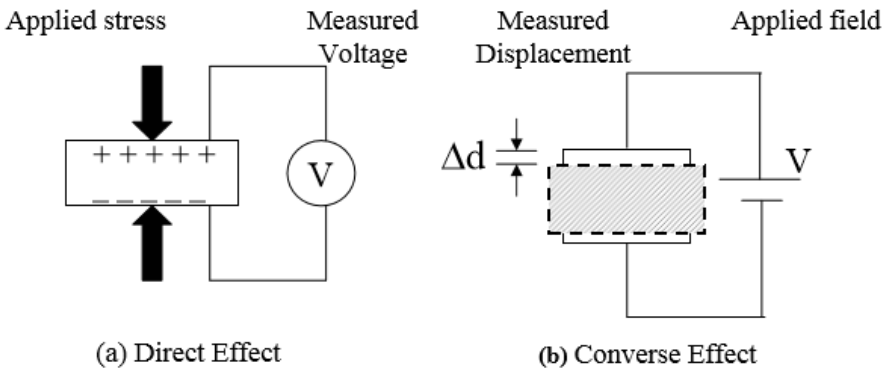

Fig 4. (a) direct piezoelectric effect (b) converse effect[22]

- **Poling direction**

Poling is the main process for material to build its PE properties. The process is to heat the substance to a temperature higher than the curie temperature in order to energise the molecules. When the molecules move freely they are to subjected to high electrical field causing the molecules to align in a single direction Fig. 5(b).

The process continues after the electric filed is removed and it allowed to cool down. The process within the unit cell structure is shown in Fig. 5(a). Once the material is compressed it results in a voltage having same polarity as the poling voltage across the electrodes. Provided the material is under tension an opposite voltage shall be produced across the electrodes[21].

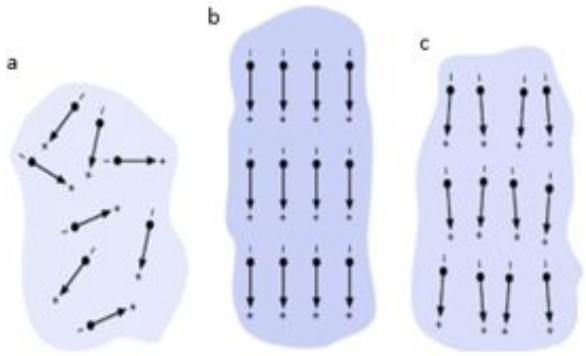

Fig 5. Electric dipoles in domains: (a) unpoled (b) during and (c) after poling[21

- **Piezoelectric strain coeficient**

The piezoelectric activity is denoted by d_{ij} and is measured in Coulomb/Newton. The d_{ij} coefficient is the electrical charge on i axis divided by $1m^2$ area when it is presented to a pressure of 1 Pa along the j axis [22].

$$d_{ij} = \frac{eletrical\ charge\ density}{applied\ stress} = \frac{Q_i/A_i}{F_j/A_j} \qquad (1)$$

Where $A_x =$ area according to x axis

$$F = force$$

$$Q = charge$$

$$d_{ij} = \frac{strain}{applied\ electrical\ field} = \frac{\Delta L_i/L_i}{V_j/L_j} \qquad (2)$$

Where $L_x = length\ according\ to\ x\ axis$ and $V = voltage$

There are two common PEH configurations, 33-mode and 31-mode, as demonstrated in Fig. 6(a) where stress is applied either along the polar axis (3-direction) or at right angles to it (1-direction). It is seen that 31-mode has large strain in the 1-direction and hence d_{31} is most desirable in VEH [22],[23].

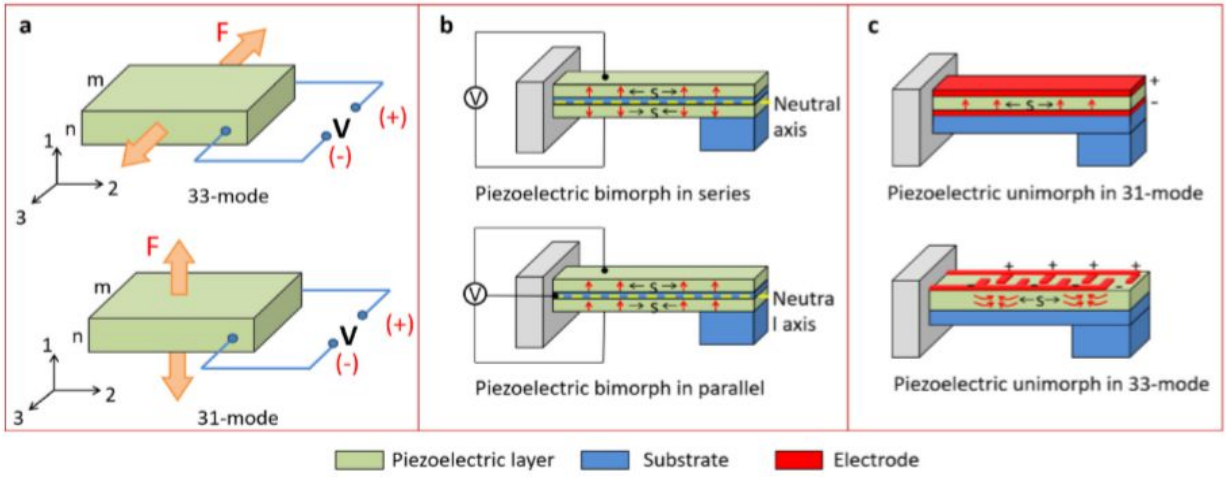

Fig 6. (a) Configuration of 33-mode and the 31-mode (b) series and parallel configurations of 31-mode bimorph cantilever (c) unimorph cantilever in 31-mode and 33-mode [4].

1.6. Bimorph, unimorph and multilayer cantilevers

Cantilever is a commonly adopted structure in PEH, mainly for VEH, typically comes in the form of bimorph or unimorph cantilevers. Vibration-based PEH with unimorph cantilevers are mostly used in applications of MEMS technology. Fig. 6(c) demonstrates 31-mode of a unimorph cantilever in which the PE layer is sandwiched between upper and lower electrodes. However, in 33-mode, the electrode is placed above the PE layer using interdigital electrodes (IDEs). The open circuit voltage V_{oc} is given as [4],

$$V_{oc} = \frac{d_{ij}}{\varepsilon_r \varepsilon_0} \sigma_{ij} g_e \qquad (3)$$

Where V_{oc} depends on applied stress σ_{ij}, the piezoelectric coefficient d_{ij}, and the gap distance between electrodes g_e, ε_r and ε_0 are the relative dielectric constant and the permittivity of vacuum, respectively. There is an example of a clamped-clamped beam structure that avoids the need for substrate material, made of PVDF unimorph producing upto 4μW from vibrations of 0.5g at 70Hz shown in Fig.7(a) [23]. Fig. 6(b) shows bimorph cantilever in 31mode, comprising of center shim having two separate PE layers on either side. The top layer of the cantilever is stretched and the bottom layer is compressed or vice versa. However, multilayer harvesters generate more than twice that obtained from bimorphs, showing better than 100% spike in performance. Rammohan et al., tested PVDF multilayer harvester that generates 230 μW/ cm^3/ $g^2$and bimorphs that generates 98 μW/ cm^3/ g^2, shown in fig 7(b)[3]. Single supply pre-biasing (SSPB) is used in multilayer harvesters for improved power generation[24]. Higher number of PE layers such as triple layer harvesters are implemented and compared with bimorphs having same total thickness [25].

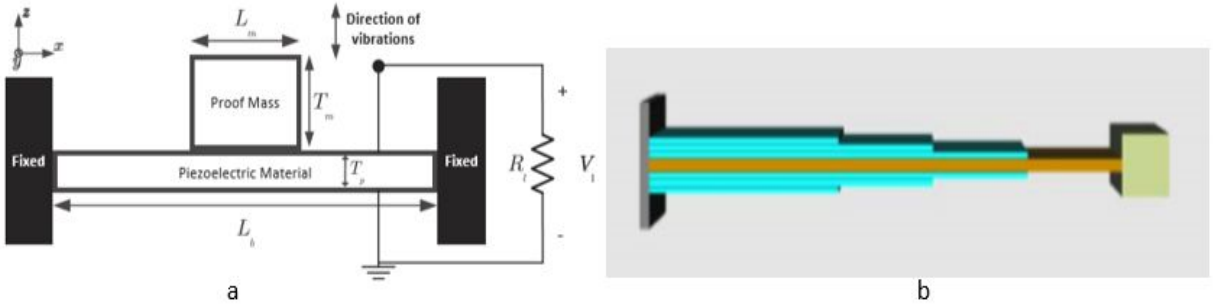

Fig 7. (a) Clamped-clamped beam structure[23] (b) Multistep Harvester structure[3]

1.7. Shapes of cantilevers

The common cantilever shape is that of a rectangule because it can be easy implemented, it is a well-understood model and most importantly has large stress distribution for any given input. However, theoretical analysis verified by experiments show that a tapered or triangular-shaped cantilevers can outperform rectangular shaped beam[26]-[29]. Kumar et al., have proven that varying the width of PVEH by using BPFs (Block pulse functions) triangular piezoelectric cantilever beams shown in Fig. 8(a) produce upto 2.5 times more result than that produced by a constant width PE cantilever. [30]
Zigzag or meandering beam-shapes shown in Fig. 8(b) reduce resonance frequency by reducing stiffness of the cantilever structure[31],[32]. Although most PVEHs use proof mass, Montazer et al., have come up with an innovative shape where the cantilever itself act as a proof mass [33].
PEH can also be seen in circular shapes. For practical cases, where energy harvester is excited randomly, a clamped circular plate energy harvester interconnected to a circular piezoelectric layer was designed to optimize the performance[34]. Kim et al., and Shi et al., [34],[35] discussed

piezoelectric circular diaphragms operating under varying pressures backed by theoretical and experimental analyses. But circular shape harvesters are relatively stiffer than rectangular cantilever so they have higher resonance frequencies.

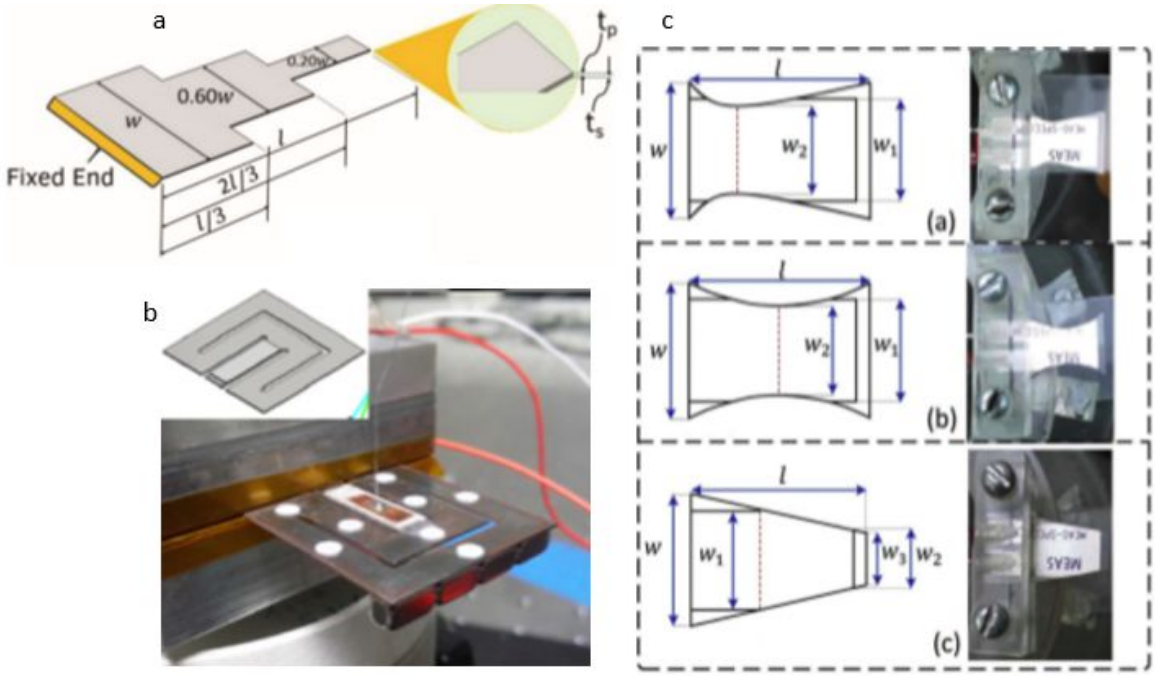

Fig 8. (a)An unimorph PEH using BPFs[30] (b) zigzag or meandering cantilever designs [31].NEWQ, HQ and Trapezoidal designs[33]

1.8. Performance enhancement methods

PVEH devices use to good advantage the facility of PE material to generate electricity in response to mechanical stimuli. However, environmental vibration have frequency limits and acceleration that are generally below the operational mode of PEH system. Therefore, output power increment and broad spectrum of operating bandwidth are much desired. A short outlook on some proven methods are discussed below.

- **Multi-degree of freedom harvesting method**

Expansion of the frequency bandwidthc can be done by inducing of an array of single-degree of freedom oscillators with unique resonant frequencies [36]. El-Hebeary et al., have proposed multi-frequency VEH stretching from 8 to 19Hz by applying a three-stage open delta-shaped plate [37]. PE plates with multiple masses attached at three different locations having compliant tri-spring structure can also improve bandwidth[38]. A detailed study to improve performance and bandwidth broadening with multiple resonant peaks is shown in [37],[38].

- **Mono-stable non linear PEH method**

A popular method to initiate a nonlinear restoring force is by using magnetic or mechanical force. The findings imply that by cautiously inducing non linearity in the system can lead to widening of the opeartion bandwidth for efficient use of random and non-stationary sources, this can be carried out by subjecting to mechanical stress, stretching, preload, stopper and magnetic force [39]-[41].

- **Frequency up conversion method**

With an eye towards facing the problem of harvesting low frequency environmental vibrations, methods like frequency up conversion(FUC) method, transforming low-frequency vibrations to high-frequency self-oscillations can help. FUC method is grouped into mechanical impact, mechanical plucking, snap-through bulking and magnetic force approaches[4]. A non-impact PEH without magnetic coupling is formed using snap-through action on a pre-buckled beam [42]. Low frequency is attained using a FUC beam-roller harvester along with multi-directional vibration in combination with a piezoelectric cantilever [43].

- **Hybrid energy harvesting mechanism**

Hybrid energy harvesting devices can help overcome the disadvantages of individual energy harvesting mechanisms. Researchers have began working on hybrid energy harvesters that can at any given moment extract energy from multiple energy sources. For instance, harvester which can be attached to a human body can use RF(radio frequency), solar and thermal energies. Son Nguyen et al., has proposed a hybrid piezoelectric and radio frequency (RF) energy harvesting system using (PVDF) for wearable devices[44].

- **Piezoelectric and electromagnetic hybrid mechanism**

High voltages and lower current is the performance characteristic of PEHs. But, electromagnetic effect yield comparatively lesser voltage but higher current due to low internal impedance. Sang et al., have constructed a typical hybrid VEH configuration shown in Fig.9(a) integrated piezoelectric and electromagnetic device made from a piezoelectric cantilever with proof mass of a magnet on the tip, a maximum power of 10.7 mW at resonant frequency with an increase of 81.4% compared to 5.9 mW is case of only electromagnetic system is seen [45].

- **Piezoelectric and triboelectric hybrid mechanism**

Triboelectric energy harvesting first proposed by Wang's group, is attracting research interest focused on harvesting low frequency energy. Vortex shedding effect is used to increase the output performance in piezoelectric and tribolelectric based wind energy harvester. Due to the breeze PVDF cantilever driven by the flapping blade deforms resulting the aluminium surface on the PVDF cantilever to make contacts with the top and bottom PDMS (Polydimethylsiloxane) surfaces as shown in Fig.9(b) [46].

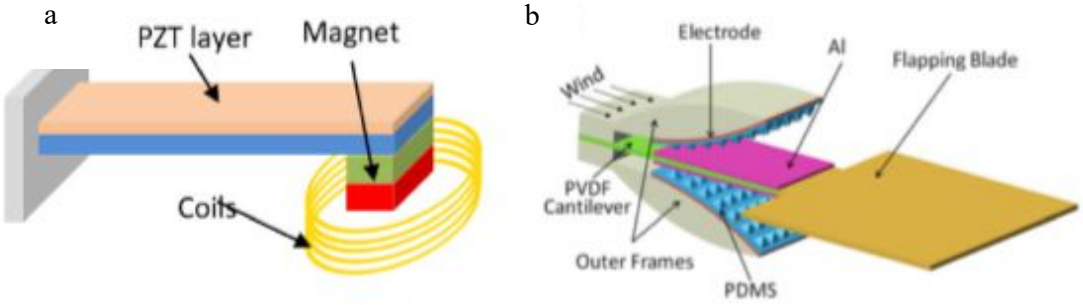

Fig 9. (a) piezoelectric and electromagnetic based hybrid system [45] (b)piezoelectric and triboelectric-based wind energy harvester[46].

1.9. Section conclusion

The preceding section presented a review of recent publications along with main theoretical concepts and principles used in the field of vibration energy harvesting. The reader was introduced to Internet of Things,"plug and forget" concept and problems in energy harvesting systems, followed by a brief review of energy conversion principles, with particular emphasize on piezoelectric energy harvesters (PEHs). Most common configurations of PEHs with their capabilities, limitations as well as areas of design improvement were elaborated. In general, this section introduced the reader to the field of energy harvesting, outlaying its basic principles, recent research achievements and commonly met issues or, in other words, presented a steady background to understand theoretical and experimental research presented in the following sections.

The following conclusions drawn are follows.

- It was decided to develope PEH for powering of wireless sensors. Due to the ubiquitous presence of mechanical vibrations in industrialized and house hold environment, mechanical vibrations were chosen as energy source in this study;
- In terms of analysed vibration to electricity conversion mechanisms, piezoelectric transduction was chosen for further research. It was selected due to high power densities, micro-scale integration ability, commercial availability of various piezoelectric materials and their ease of adaptation for different harvester configurations;
- The PE material most suitable for our harvester is PVDF because of its higher tensile strength, lower stiffness and its ease of integration in manufacturing processes;
- As of different PEH configurations studied, cantilever type PEH operating in d31 mode was chosen for further research. It was selected due to ease of fabrication, ability to adapt to resonant frequency of device and intrinsic dynamic response characteristics;
- After studying unimorph and bimorph configurations, multilayer PVEH in parallel configuration is adopted in proposed harvester;
- Analyses on the influence of cantilever shape reveals during bending the stress is highest at the clamped end and lowest at the free end, so the proposed PVEH is designed with cantilever having longer width compared to length;
- It was also decided to firstly implement finite element modelling technique in order to thoroughly understand performance of PEHs – i.e., the way performance of PEH is affected when one is changing dimensions and shape of PVEH, tipmass and gap parameters, introducing rigid support to PEH configuration or connecting PEH to simple electric circuit;
- Moreover, optimization of device using tipmass and gap adjustment was chosen as the main ground to perform experimental studies and verify simulation results;
- As of different PVEH performance enhancement methods discussed it was decided to optimize geometric parameters and shape of PEH cantilever substrate as well as to incorporate mechanical supports to PEH configuration;

2. Theoretical calculations

Before entering into the experimental investigation domain, it is important to have clear apprehension of the theoretical and mathematical aspect behind it. This sections gives the calculations and formulas used in this research.

2.1. Governing Equations for Piezoeletricity

The fundamental calculation derived from the tensor expression for PE effect caused by 1 dimension mechanical disfiguration is given below[47]:

$$D_3 = d_{31}T_1 + \varepsilon_{33}^T E_3 \quad (4)$$

Where D_3 is electrical displacement; d_{31} is piezoelectric constant; T_1 is axial stress component, ε_{33}^T is the permittivity component at constant stress, and E_3 is the electrical field component. Subscripts 1 and 3 denote the longitudinal direction and the poling direction, respectively (Fig 12). In case the external electrical field is absent (E_3= 0), the equation is equal to:

$$D_3 = d_{31}T_1 = d_{31}E_pS_1 \quad (5)$$

where $S_1$is the bending strain, E_p is the Young's modulus of the PVDF layer.

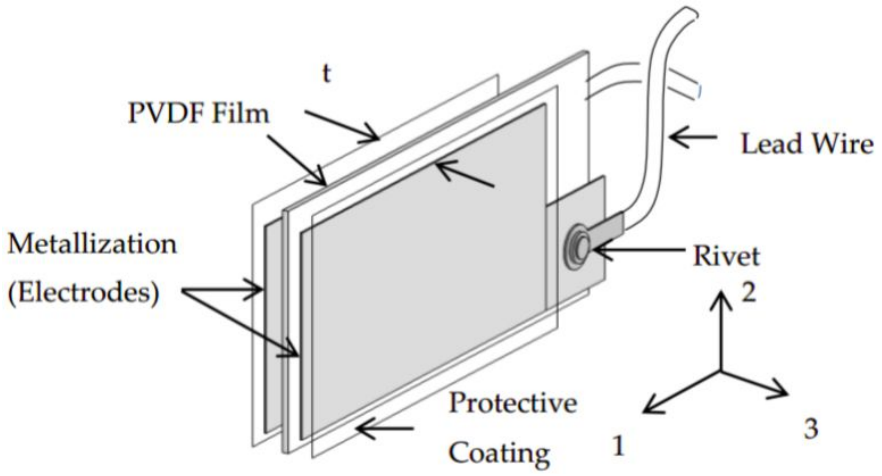

Fig 10. Schematic configuration of PVDF sensor [48]

2.2. Mechanical and electrical properties

The commercial PECs used in the investigation are multilayer stack of PE films from Measurement Specialties, the PVDF is layered between 2 Ag (silver) electrodes and a polyester (PET) layer laminate is at the bottom of the electrode and a very thin layer of acrylic laminate is on the top of the cantilever as shown in Fig. 11. Since thickness of PET and acrylic is not the same, the top and bottom side of the neutral axis will be asymmetric.

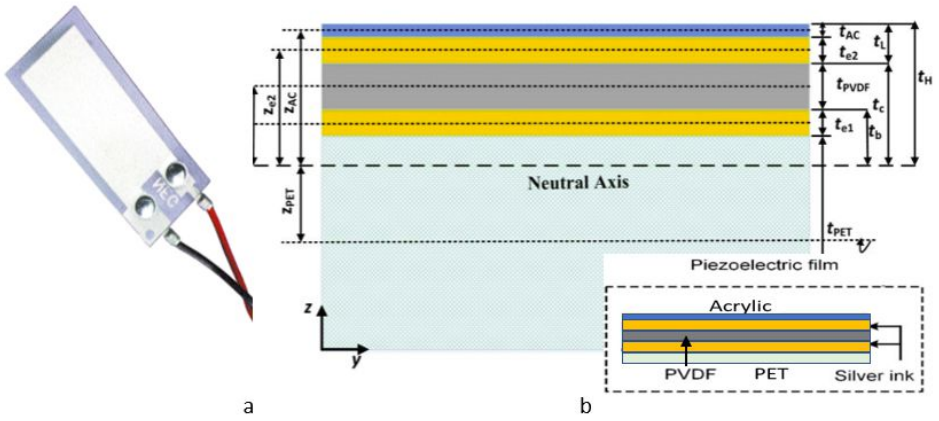

Fig 11. (a) Sample cantilever used in this study (b) cross section view of the different layers [33]

Since the entire substrate area is not covered by the piezoelectric or electrode layers, mass per unit length is [33],

$$m(x) = b(x)\rho_{PET}t_{PET} + y(x)\rho_{e1}t_{e1} + y(x)\,\rho_{PVDF}t_{PVDF} + y(x)\rho_{e2}t_{e2} + b(x)\rho_{AC}t_{AC} \quad (6)$$

Where $m(x)$ is mass per unit length of the substrate ; ρ_{PET}, ρ_{e1}, ρ_{PVDF}, ρ_{e2} and ρ_{AC} are the densities of the 5 layers ; t_{PET}, t_{e1}, t_{PVDF},, t_{e2} and t_{AC} are the thickness of the substrate, lower electrode, piezoelectric material, top electrode and protect the layer of acrylic, respectively. The electrical and the mechanical properties of the material are listed in Table below. E_{PET}, E_{e1}, E_{PVDF}, E_{e2} and E_{AC} are the modulus of elasticity of the composite layers.

Table 1. Mechanical and electrical properties of commercial PEHs[33]

Material	Mechanical and Electrical properties	
Polyvinylidene fluoride (PVDF)	Piezoelectric constant	$d_{31} = 23 \times 10^{-12} CN^{-1}$
	Relative Permittivity	$\varepsilon_r = 16$
	Young's modulus	$\varepsilon_p = 2 - 4GPa$
	Poisson's ratio	$v_p = 0.35$
	Density	$\rho_p = 1780(Kg/m^3)$
Polyester (PET) Mylar	Young's modulus	$E_{PET} = 1.4GPa$
	Poisson's ratio	$v_{PET} = 0.4$
	Density	$\rho_{PET} = 930(Kg/m^3)$
Silver(Ag)	Young's modulus	$E_e = 69GPa$
	Poisson's ratio	$v_e = 0.37$
	Density	$\rho_e = 10500(Kg/m^3)$
Acrylic	Young's modulus	$E_e = 3.9GPa$
	Poisson's ratio	$v_e = 0.4$
	Density	$\rho_e = 1190(Kg/m^3)$

2.3. Problem of Imdepence mismatch

PE materials have internal impedances,so some power generated by the PVDF is dissipated due to this effect. PVDF harvester behaves as an AC voltage source with an internal impedance.It will be seen in further chapters this internal impedance is inversely proportional to frequency. Also an

impedence mismatch will worsen the problem of energy dissipation. Hence ie is very important to have a proper impedence matching between the input and output. A basic electrical impedance-matching circuit needs one capacitor and one inductor as shown in the fig 12, R_1 is the source impedance and R_2 is the load impedance. X_1 is the input capacitive reactance X_c and X_2 must be an inductive reactance. Capacitive reactance X_c is in parallel with the source and X_2 is in series with the load[50],[51].

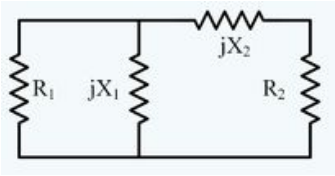

Fig 12. Basic schematic for Impedance matching

Taking into consideration source impedance of R1 and load impedance R2, if the reactance is in parallel with the source impedance, the combined impedance can be written as,

$$\frac{jR_1C}{R_1+jX_1} \qquad (7)$$

If series reactance is cancelled by the imaginary part of the above impedance, the real part becomes,

$$R_2 = R_1\left(\frac{X_1}{R_1+X_1}\right) \qquad (8)$$

$$X_1 = X_c = \frac{1}{2\pi fC} \qquad (9)$$

$$R_1 = R_2\frac{X_c}{(X_c - R_2)} \qquad (10)$$

For maximum power, R_2 value should be equal to the internal resistance of PVEH.

2.4. Calculation of Internal resistance and internal voltage

In order to calculate internal resistance of a piezoelectric harvester experiment data is necessary, most importantly open circuit output voltage and load peak to peak voltage is needed. Two cases of experiments are considered. The experiment circuit used is shown in fig 13. Firstly in case (a) the cantilever open circuit output voltage V_1 is recorded when no test resistance is connected to the cantilever, only the oscilloscope load impedance R_{os} acts as the load in first case. In the second case a test resistance R_t is connected to the cantilever, since R_{os} and R_t are connected in parallel, an effective resistance R_p is applied, the peak to peak voltage output measured in this case is V_2.

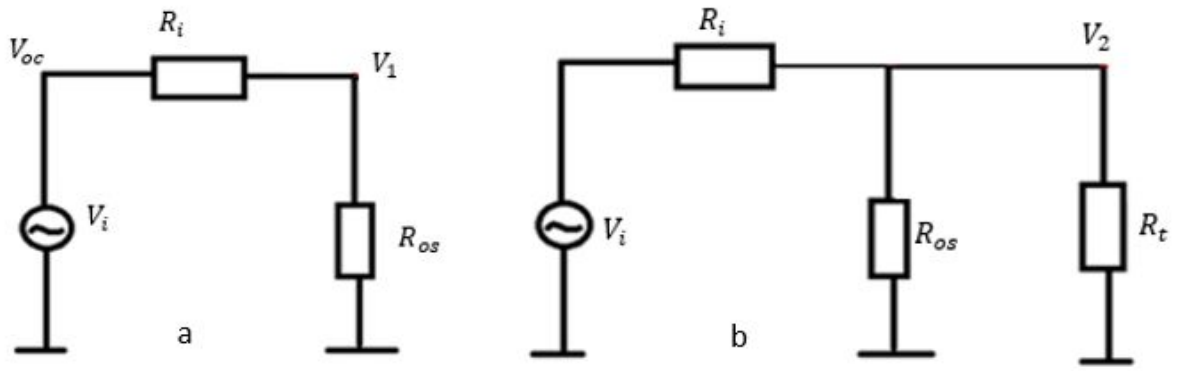

Fig 13.(a) no load circuit (b) circuit connected to test resistance

Therefore, the current generated in circuit (a) will be,

$$I_1 = \frac{V_i}{R_i + R_{os}} \quad (11)$$

From ohm's law,

$$V_1 = I_1 \times R_{os} \quad (12)$$

$$V_1 = \frac{V_i R_{os}}{R_i + R_{os}} \quad (13)$$

Similarly, for circuit (b),

$$I_2 = \frac{V_i}{R_i + R_p} \quad (14)$$

$$R_p = \frac{R_{os} R_t}{R_{os} + R_t} \quad (15)$$

$$V_2 = \frac{V_i R_p}{R_i + R_p} \quad (16)$$

Simplying equation (13) and (16) it is reduced to,

$$V_i = \frac{V_1 V_2 (R_{os} - R_p)}{R_{os} V_2 - V_1 R_p} \quad (17)$$

$$R_i = \frac{R_p (V_1 R_{os} - R_{os} V_2)}{R_{os} V_2 - V_1 R_p} \quad (18)$$

The derived equation (18) is used to calculate the internal resistance of different piezoelectric cantilever samples used in this study

2.5. Maximum theoretical power output

The maximum theoretical output of the different cantilevers helps to estimate the cantilever potential. The following equations are derived so that the measured cantilever output can be compared with its maximum achievable ouput. In fig 15 (a), the current output is equal to,

$$I = \frac{V_{oc}}{R_i + R_{os}} \quad (19)$$

Where V_{oc} is internal voltage of cantilever , shown in fig13 (a). With $R_i = R_{os}$ current is reduced to,

$$I = \frac{V_{oc}}{2R_i} \quad (20)$$

The voltage drop between V_c and V_1 is given by,

$$V_c - V_1 = IR_i = \left(\frac{V_1}{R_{os}}\right) R_i \quad (21)$$

$$V_c = \left(\frac{V_1}{R_{os}}\right) R_i + V_1 \quad (22)$$

When $R_L = R_i$ maximum power is given by,

$$P_{max} = V_{oc} \times I = \frac{V_{oc}^2}{2R_i} \quad (23)$$

$$\int_0^T P_{max}(t) = Energy \quad (24)$$

By integrating equation (23) over input time period, energy is obtained. Equation (23) and (24) are used to calculate maximum power and maximum energy generated by the investigated piezoelectric cantilevers. The electrical power determined shows the upper limit of the electrical power deliverable by a PE cantilever. In the next section, different parameters of cantilever performance are explored and analysed. The above formulated equations were used for comparative study of different cantilevers and helped draw conclusions that promoted the development and construction of proposed PVDF harvester device.

3. Tests on actuator

Actuator is the main device that was used to excite the cantilever, so it was essential to first understand the behaviour of the actuator under different circumstances.

3.1. Actuator calibration

The actuator used in this study was calibrated to ensure that there is no confusion in the quantity of input supplied. The acceleration produced by the actuator is not the same for all input frequencies. Since acceleration is different for each input frequency, acceleration becomes a function of input supply frequency. Hence it is important to calibrate the actuator in such a way that the input frequency is taken in account. A digital ICP accelerometer and an analog accelerometer are used to calibrate the actuator with respect to the input supply frequency, input voltage provided to the actuator coil for excitation (V_{CV}) and acceleration voltage (V_{AV}) of analog acclerometer. The experiment setup is shown in fig 14(a). Paraffin wax is used to mount the analog and digital accelerometers on the actuator diaphragm as shown in fig 14(b). Power supply is given to the signal generator and amplifier which provides a random input to the coil terminals of the actuator (V_{CV}) maintained at 0.2V, while the input frequency is varied from 10Hz to 60Hz. At an interval of every 5 Hz, the following readings are noted:-input supply frequency F(Hz), peak to peak acceleration voltage (V_{AV}) displayed on oscilloscope and actual acceleration excitation (Acc) measured by ICP digital accelerometer displayed on the computer interface in g units. The readings are shown in Table 2.

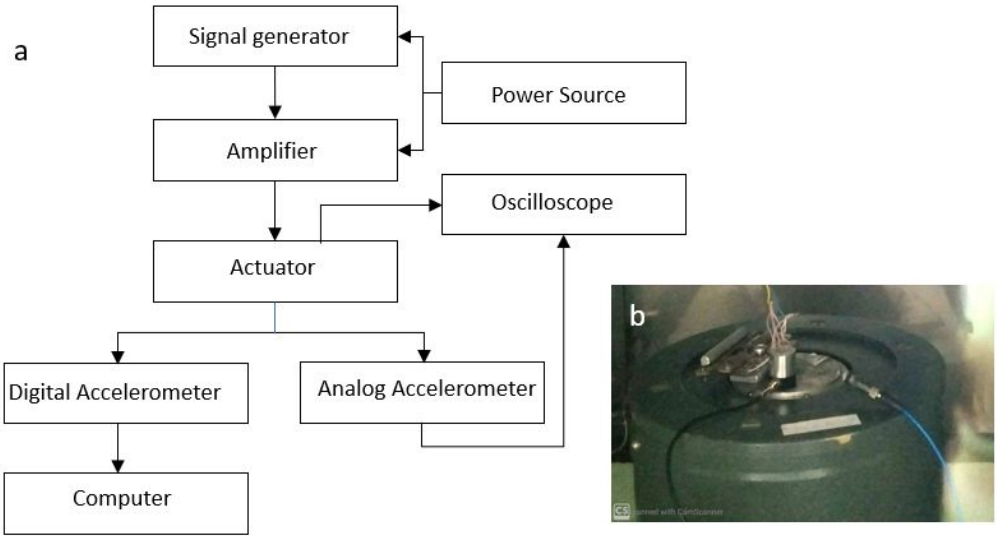

Fig 14. (a)Structure of experiment system. (b) Digital and analog accelerometer mounted on the actuator diaphragm.

Table 2. Calculation of acceleration coefficients

F(Hz)	$V_{AV}(V)$	Acc (g)	$A_{Coeff_{CV}}$	$A_{Coeff_{AV}}$ (g)
15	0.007	0.053	0.051	0.050
20	0.009	0.063	0.071	0.066
25	0.012	0.082	0.091	0.096
30	0.013	0.111	0.111	0.111

35	0.014	0.147	0.131	0.122
40	0.017	0.158	0.151	0.155
45	0.018	0.167	0.171	0.166
50	0.020	0.196	0.191	0.189
55	0.022	0.229	0.211	0.215
60	0.022	0.216	0.231	0.226

The readings are used to form a relationship between V_{CV}, V_{AV} and Acc such that any one of these parameters can help find the other parameters. Coefficient of analog accelerometer($Coeff_{AV}$) defines the relation between V_{AV} and Acc.

$$Coeff_{AV} = \frac{Measured\ acceleration\ (g)}{Analog\ acclerometer\ voltage\ (V_{AV})} \qquad (25)$$

By ploting $Coeff_{AV}$ over input frequency, a trendline equation is obtained as shown fig 14 (b).

$$Coeff_{AV} = 0.0621 \times\ frequency(Hz) + 6.4451 \quad (26)$$

The product of this coefficient and V_{AV}, gives acceleration of actuator.

$$A_{Coeff_{AV}}\ (g) = Coeff_{AV}\ \times V_{AV} \qquad (27)$$

Equations (26) and (27) can be used to calculate acceleration with respect to input frequency supplied, when the analog acceleration voltage is known. Likewise, coefficient of coil excitation voltage ($Coeff_{CV}$) defines the relation V_{CV} and Acc.

$$Coeff_{CV} = \frac{Measured\ acceleration(g)}{Actuator\ input\ terminal\ voltage\ (V_{CV})} \qquad (28)$$

$$Coeff_{CV} = 0.02 \times\ frequency(Hz) - 0.043 \quad (29)$$

$$A_{Coeff_{CV}}\ (g) = Coeff_{CV} \times V_{CV} \qquad (30)$$

Equations (29) and (30) can be used to calculate acceleration with respect to input frequency supplied provided V_{CV} value is known.

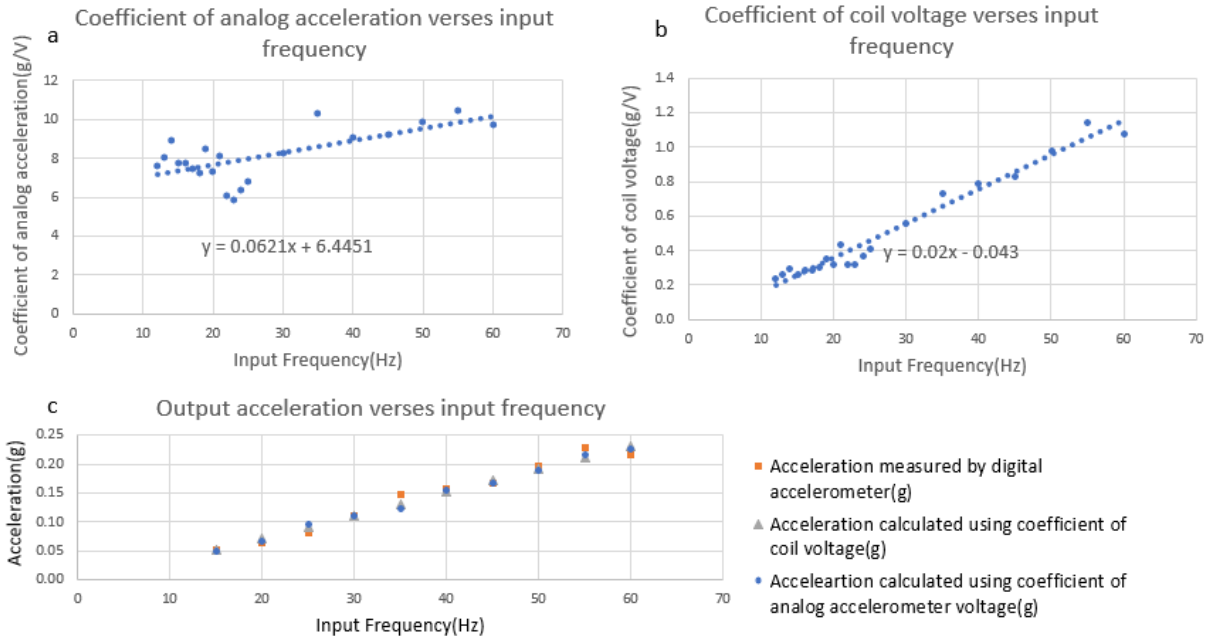

Fig 15.(a)Trendline equations for Coeff-CV (b) Trendline equations for Coeff-AV (c)Plot of measured acceleration and calculated acceleration showing close resemblance.

The deviation between calculated acceleration value and actual acceleration measured is $\pm 1\%$, hence with proposed equation and coefficients the acceleration produced by the actuator can be found when the coil excitation voltage or the analog accelerometer voltage is known.

3.2.Effect of mass on actuator performance

In order to inspect the influence of weight of object mounted on the actuator on the exciter performance, six values of weights 27gm, 37gm, 47gm, 57gm,67gm and 74gm were mounted on the actuator and frequency was varied ranging from 10Hz to 60Hz. For each weight frequency response of the exciter is plotted with respect to V_{CV} measured at the exciter input terminals so that a constant output acceleration of 0.2g is maintained. The V_{CV} value required for each weight is noted as shown in table 3. V_{27gm}, V_{37gm}, V_{47gm}, V_{57gm}, V_{67gm} and V_{74gm} are V_{CV} values for the different weights mounted on the exciter.

Table 3. Table of coil excitation voltage values for different weights mounted on actuator at constant acceleration

f(Hz)	$V_{27gm}(V)$	$V_{37gm}(V)$	$V_{47gm}(V)$	$V_{57gm}(V)$	$V_{67gm}(V)$	$V_{76gm}(V)$
10	2.1	2.24	2.24	2.2	2.12	2.17
20	0.84	0.8	0.84	0.81	0.74	0.79
30	0.5	0.45	0.48	0.47	0.44	0.44
40	0.34	0.32	0.32	0.33	0.33	0.34
50	0.232	0.25	0.25	0.28	0.24	0.25
60	0.224	0.24	0.24	0.26	0.25	0.232

V_{CV} is plotted for the respective weights, shown in Fig 16(a). For every 10gms increase in weight mounted on the actuator there is hardy any change in the coil excitation voltage requirements. Hence it is clear that mass has no significant effect on the actuator performance. However, at lower frequencies the actuator requires more input to maintain same acceleration performance as seen in fig 16(a). V_{CV} requirement at 10Hz is 10 times more than what is required at 60 Hz. There is an exponential increase in the input requirement as the frequency decreases, seen in fig 16(b). The coil input requirement at 10 Hz is 3 times of what is required at an input frequency of 20 Hz. This could mean that actuator is not meant to function below 20 Hz frequency.

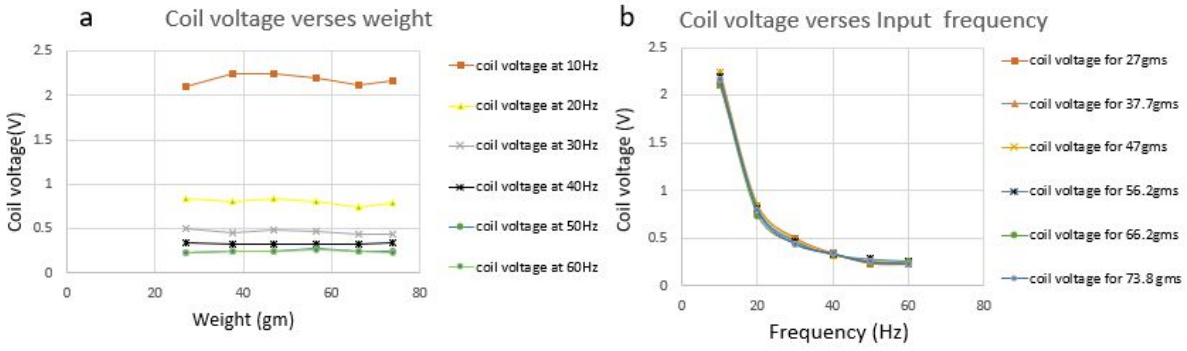

Fig 16. (a) Plot of coil excitation voltage requirements for different masses (b) Frequency response of each weight mounted on the actuator under constant 0.2g acceleration.

4. Initial considerations

The experiment described here is of an initial nature, where even the qualitative outcome was not known a priori. The purpose was to discover areas of interest for further investigations, where focus could be directed to specific issues. Some of the considerations prior to designing the experiments are discussed here like finding suitable pulse width of input so as to obtain a better output.

4.1.Varying input pulse width

The experiment set up is as shown in block diagram Fig.14(a), V_{CV} measured in every experiment and input supply frequency value is sufficient to calculate acceleration using equation (29) and (30). The actual experimental setup is given in Fig.17. The PE cantilever from MEAS is mounted on the actuator, power supply is given to the signal generator and amplifier which provides a pulse input to the coil terminals of the actuator. An oscilloscope is used to record the open circuit output voltage of the cantilever and input V_{CV}.The pulse width of the input signal has to be adjusted such that the cantilever and the actuator move with maximum resonance. Pulse width of 10ms showed better results than 5ms, 12ms, 15ms or 20ms pulse widths.

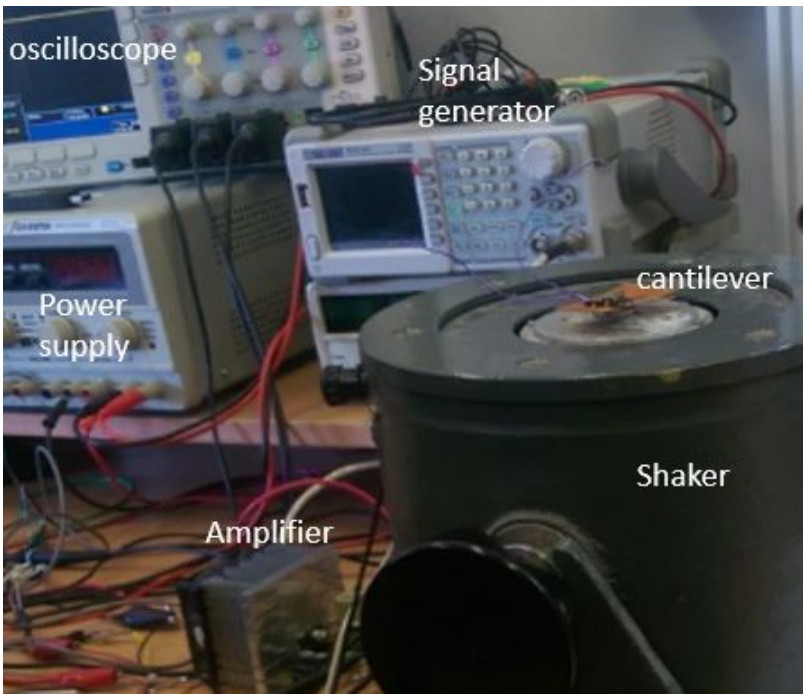

Fig 17. Photo of actual experiment set up

4.2.Calculation of internal resistance, power and energy for a cantilever

A pulse input signal of 1V peak to peak coil excitation voltage is provided to the actuator as shown in Fig 18.(a). The experiment set up is shown in Fig.17. In order to calculate power generated by a cantilever, its internal resistance should be known. To calculate internal resistance(R_i), the output peak to peak voltage should be known. The output for a pulse input is shown in Fig 18.(b). Since the first three peaks are distorted, the 4th peak to peak voltage value is considered for calculation of the internal resistance.

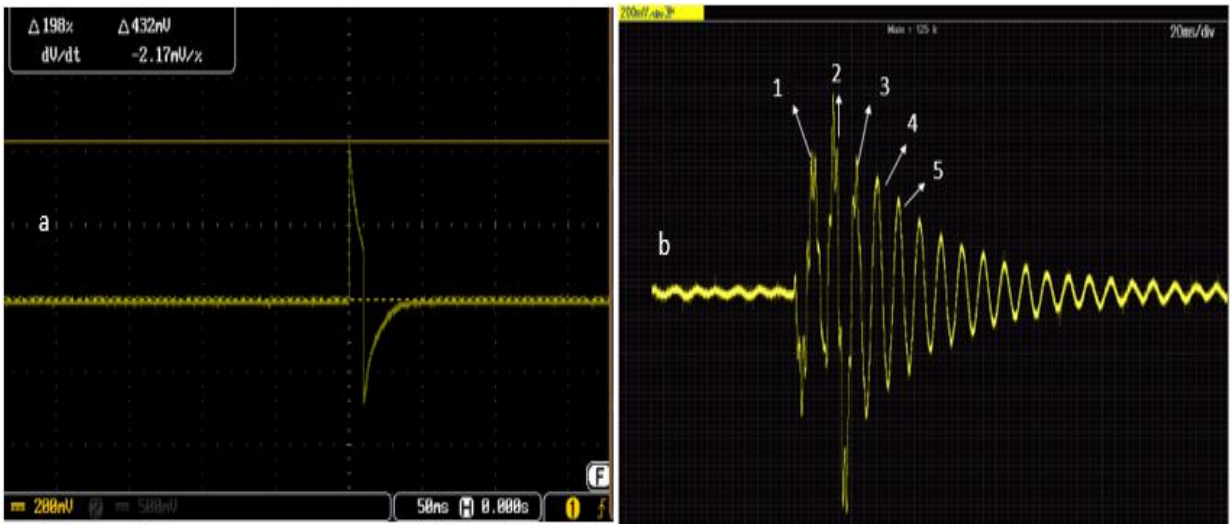

Fig 18. (a) pulse input of 1Vpp (b) Open circuit voltage of cantilever

The open circuit voltage V_1 for the first five peaks in noted down from the oscilloscope. Similarly, experiment is repeated by connecting a test resistance of $10M\Omega$ and V_2 (peak to peak voltage across the test resistance) is noted down. Any one of the first few sinosoidal voltage peaks can be considered to calculate R_i, provided the same n^{th} number of peak to peak voltage is considered in both cases- without test resistance and with test resistance. The readings taken as shown in table 4.

Table 4. Cantilever output for circuit (a)without test resistance and (a)with test resistance

n^{th} peak	$V_1(V)$	$V_2(V)$	V_1/V_2
1	0.790	0.760	1.039
2	0.820	0.800	1.023
3	1.080	1.018	1.058
4	0.742	0.714	1.039
5	0.580	0.553	1.047

The ratio of V_1/V_2 is almost constant. The chosen V_1 value is 0.742V; V_2 is 0.760; R_{os} is $10M$; R_t is $10M\Omega$; hence R_p is $5M\Omega$. After substituting these values in equation (18) internal resistance is obtained.

$$R_i = \frac{5 \times 10^6 \times (0.742 \times 10 \times 10^6 - 10 \times 10^6 \times 0.714)}{(10 \times 10^6 \times 0.716 - 0.742 \times 5 \times 10^6)}$$
$$= 408163.26\ \Omega$$
$$\sim 0.4M\Omega$$

Once the internal resistance is known, it is simple to calculate maximum power and energy using microsoft excel. Power is calculated from the simple relation, P=$V^2/2R_i$ and energy is the integration of power over time. The calculation of power and energy is shown in table 5. The output curves of voltage, power and energy are shown in Fig.19

Table 5. Power and energy calculations for pulse input

n	$Time(s)$	$V=\frac{V_1}{n}\ (V)$	$Power(pW) = \frac{V^2}{2 \times 0.4 \times 10^6}$	$E(pJ) = \sum_{i=1}^{n} E_{[n-1]} + P_{(n)}$
1	1.6×10^{-6}	1.13×10^{-3}	1.59×10^{-5}	1.59×10^{-5}
2	3.2×10^{-6}	1.45×10^{-3}	2.63×10^{-5}	4.23×10^{-5}
3	4.8×10^{-6}	1.94×10^{-3}	4.68×10^{-5}	8.91×10^{-5}
n	1×10^{-1}	1.1×10^{-3}	1.59×10^{-5}	584.008

Where n is the total number of signal points considered.

Energy verses time graph is obtained by adding consecutive power over time. As seen in the table 5 and in fig 19(c), energy generated is approximately 0.6 nJ showing that there is need for optimization to obtain better results.

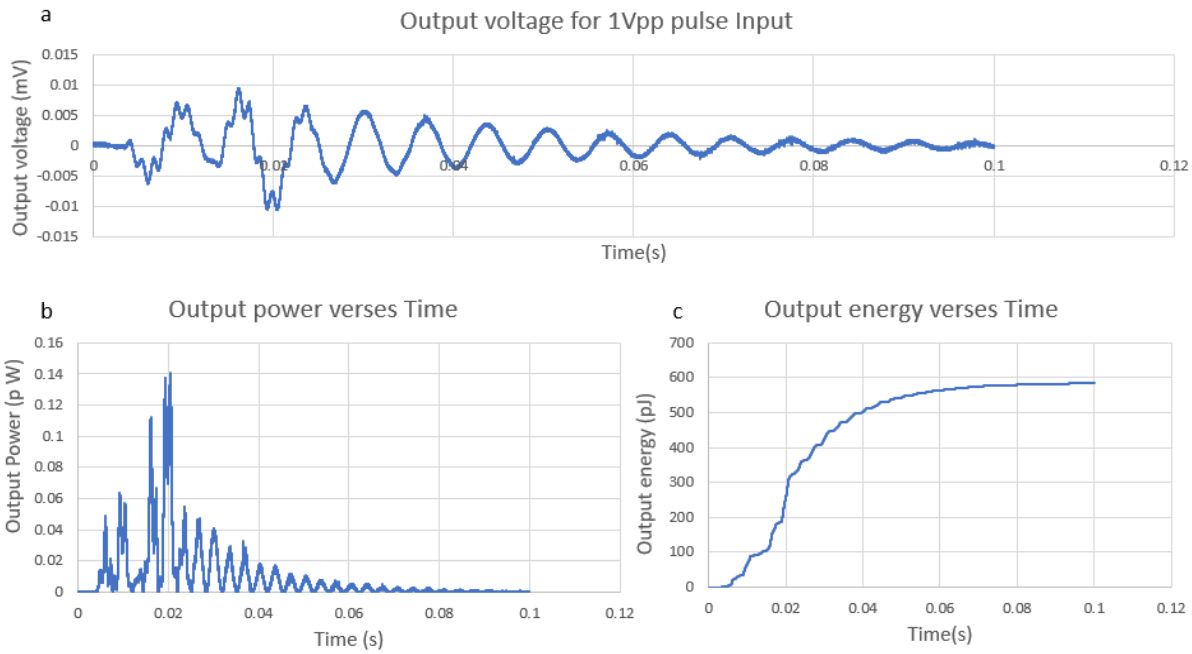

Fig 19. (a)output voltage for 1 V p-p coil excitation voltage input (b)plot for power (c) plot for energy

4.3. Interfacing circuit

A typical PVEH system is comprises of four parts: source of vibration, a piezoelectric energy converter, an interfacing circuit to rectify the generated AC voltage into DC voltage, an energy storage device such as a supercapacitor to store energy for intermittent use. The equivalent electromechanical scheme of the setup used in this study is shown in Fig 20.

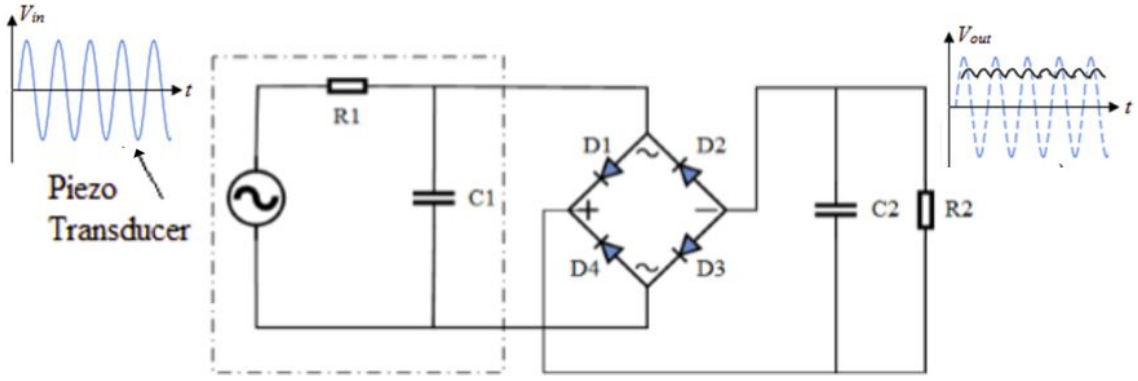

Fig 20. The electromechanical circuit of PVEH.

Although studies have indicated that a right interface circuit could increase the energy output of PE harvester, from the reviewed papers, the interface circuits of all of the vibration energy harvesters were simply resistive loads. In this study, efforts on optimizing the circuit efficiency η was done on finding the optimum load resistance and building a fairly efficient rectifier diode bridge.

In this study, four Schottky SMD diodes case number SOT23-6-1 were used to form a full- bridge rectifier, 1nF capacitor is used as C_L shown in Fig.23(b). Schottky diodes are used instead of conventional silicon diodes in order to reduce voltage drop. In forward bias, schottky diodes have drop of 0.2V to 0.3V but silicon diodes have a voltage drop of 0.6V to 1V at high voltages. As seen in fig 20, full wave bridge rectifier uses two diodes in series for every period. Current passes through diode D1, load R2, diode D3 and back to generator in one period, in the next period another route through diode D4, load, D2 and generator is taken. Since two diodes are employed in every period, total voltage drop would be 0.4V to 0.6V which is much better than 1.2V in case of silicon diodes. Hence using schottky diodes has resulted in a much smaller voltage drop.However, a better option would be the use of field effect transisters(FETs) which can totally avoid voltage drop on rectifer circuit. Rectifier efficiency for different input accelerations is shown in Fig 21(a). This interfacing circuit is suitable for practical implementation. It will be seen in the following sections that with such power-transfer circuit, the output power is relatively near to the theoretically achievable maximum power.

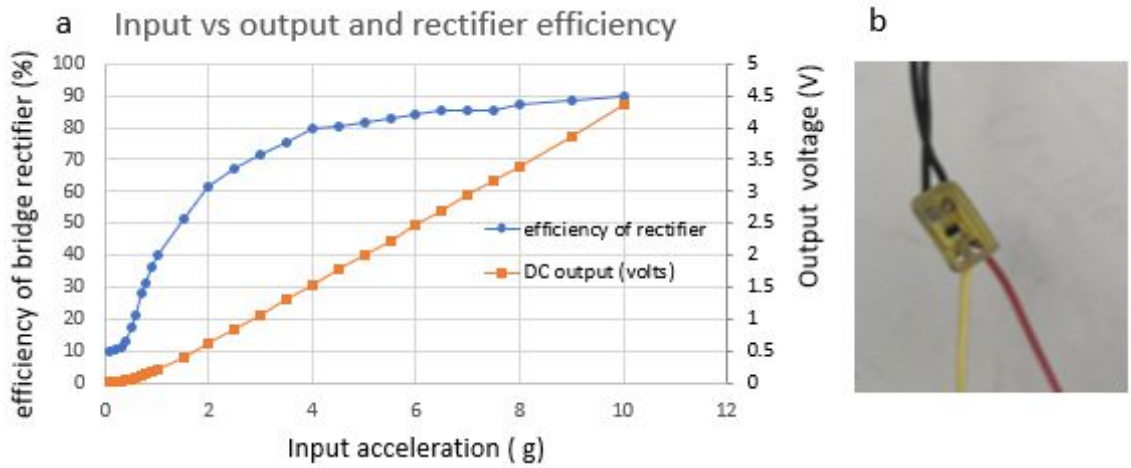

Fig 21. (a)output and efficiency of interfacing circuit (b) Photo of rectifier diode used

5. Investigation on commercial cantilevers

This sections deals with the experimental invesigation conducted on commercial cantilevers. In order to be able to predict the influence of factors like tipmass, gap and size of cantilevers various experiments were conduced on ready made cantilevers that helped in the design of real PVEHs discussed in the next chapter.

5.1. Factorial analysis on tipmass and size of cantielever

To understand the effect of tipmass and cantilever size,a set of factorial experiments were performed and statistically analyzed using Minitab software. Two unimorph cantilevers from MEAS measuring dimensions 25x 13xO.205 mm^3 and 17.8x7x0.205 mm^3 is used for this analysis. Two tipmasses of 0.3g and 0.8 g were used and both cantilevers were excited with and without the tipmass. By performing minimum number of experiments on different size cantilevers, the influence of tipmass and size was found using factorial effect. The output voltage and resonant frequency were noted for both cantilevers measured with and without the tipmass as shown in Table 6. Factor A is size of cantilever and factor B is tipmass on cantilever. Longer cantilever produced 20% more output voltage than the shorter cantilever. In Fig. 22(c), the minitab factorial analysis shows that an increase in size or volume of PVDF film and a heavier tipmass have approximately the same effect on the cantilever. The output obtained when the cantilever size is increased more than twice is equal to output obtained when twice heavier tipmass is used. This could possibly mean that rather than increasing the cantilever size one could add more tipmass to obtain better results.

Table 6. Factorial analysis input values extracted from practical experiment

Factor A	Factor B			
	tipmass low(-B)		tipmass low(+B)	
	V_{p-p}	$f_{res}\ (Hz)$	V_{p-p}	$f_{res}\ (Hz)$
Size low(-A)	1	60.9	1.2	40
Size high (+A)	1.2	50.7	1.1	41.5

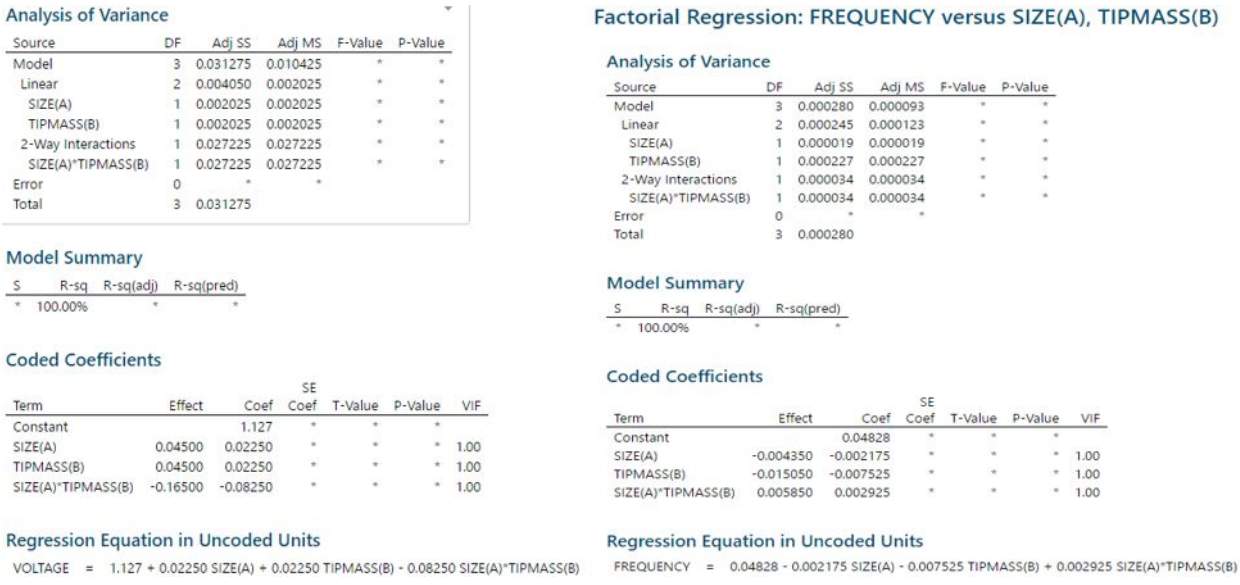

Analysis of Variance

Source	DF	Adj SS	Adj MS	F-Value	P-Value
Model	3	0.031275	0.010425	*	*
Linear	2	0.004050	0.002025	*	*
SIZE(A)	1	0.002025	0.002025	*	*
TIPMASS(B)	1	0.002025	0.002025	*	*
2-Way Interactions	1	0.027225	0.027225	*	*
SIZE(A)*TIPMASS(B)	1	0.027225	0.027225	*	*
Error	0	*	*		
Total	3	0.031275			

Model Summary

S	R-sq	R-sq(adj)	R-sq(pred)
*	100.00%	*	*

Coded Coefficients

Term	Effect	Coef	SE Coef	T-Value	P-Value	VIF
Constant		1.127	*	*	*	
SIZE(A)	0.04500	0.02250	*	*	*	1.00
TIPMASS(B)	0.04500	0.02250	*	*	*	1.00
SIZE(A)*TIPMASS(B)	-0.16500	-0.08250	*	*	*	1.00

Regression Equation in Uncoded Units

VOLTAGE = 1.127 + 0.02250 SIZE(A) + 0.02250 TIPMASS(B) - 0.08250 SIZE(A)*TIPMASS(B)

Factorial Regression: FREQUENCY versus SIZE(A), TIPMASS(B)

Analysis of Variance

Source	DF	Adj SS	Adj MS	F-Value	P-Value
Model	3	0.000280	0.000093	*	*
Linear	2	0.000245	0.000123	*	*
SIZE(A)	1	0.000019	0.000019	*	*
TIPMASS(B)	1	0.000227	0.000227	*	*
2-Way Interactions	1	0.000034	0.000034	*	*
SIZE(A)*TIPMASS(B)	1	0.000034	0.000034	*	*
Error	0	*	*		
Total	3	0.000280			

Model Summary

S	R-sq	R-sq(adj)	R-sq(pred)
*	100.00%	*	*

Coded Coefficients

Term	Effect	Coef	SE Coef	T-Value	P-Value	VIF
Constant		0.04828	*	*	*	
SIZE(A)	-0.004350	-0.002175	*	*	*	1.00
TIPMASS(B)	-0.015050	-0.007525	*	*	*	1.00
SIZE(A)*TIPMASS(B)	0.005850	0.002925	*	*	*	1.00

Regression Equation in Uncoded Units

FREQUENCY = 0.04828 - 0.002175 SIZE(A) - 0.007525 TIPMASS(B) + 0.002925 SIZE(A)*TIPMASS(B)

Fig 22. Minitab factorial analysis for voltage and frequency

The two way interaction is a combined effect of factors A and B. The interaction values for output voltage are high calculated by minitab are show in Fig. 22 (a), which means that the combined influence of having longer size cantilever and a heavier tipmass has higher impact on the cantilever than using a longer size or a heavy tipmass alone.

It is evident that there is reduction in resonant frequency with increase in tipmass, shown in Fig. 22 (d). Since the slope for tipmass is more, there is a more influence of tipmass on the resonant frequency compared to the impact of cantilever size. In other words tipmass has a greater effect on resonant frequency than on the output of the cantilever. With this analysis, it is understood that it is more important to inspect the effect of tipmass to find optimal tipmass value rather than focusing on size of cantilevers.

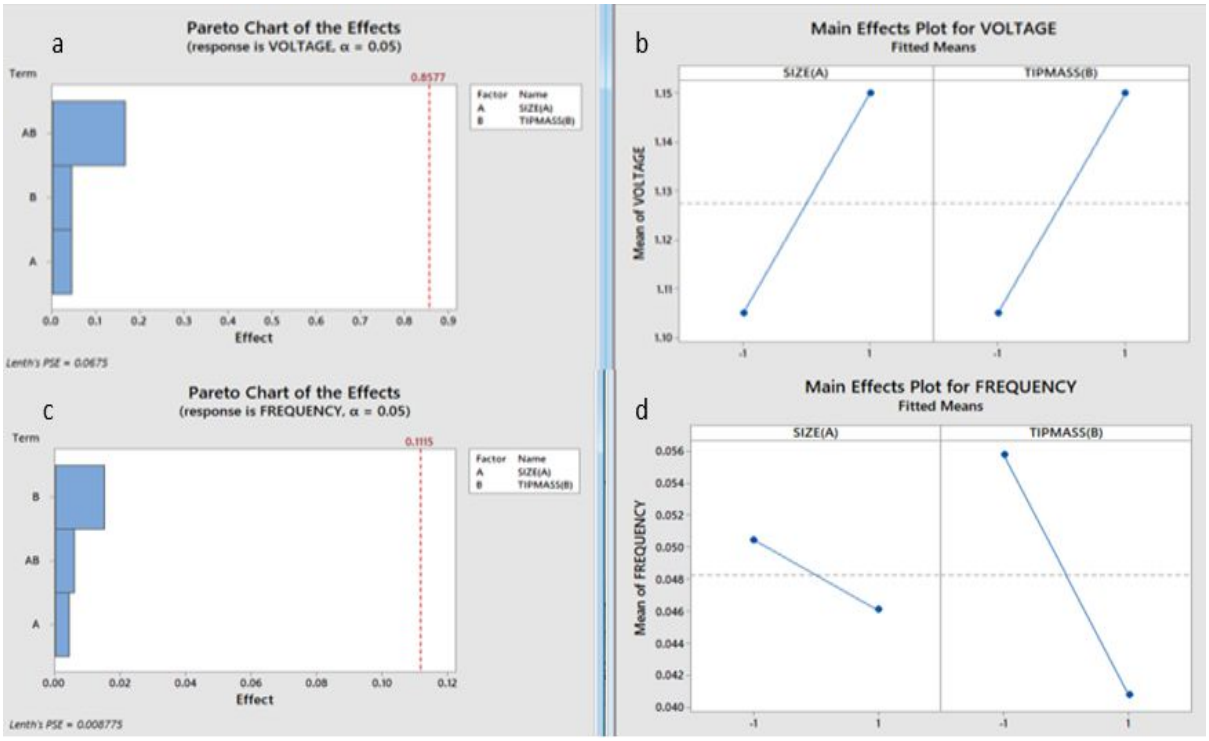

Fig 23. Minitab factorial analysis results (a) main and interaction effect of size and tipmass on output voltage (b) Main effect plot on output voltage (c) main and interaction effect of size and frequency on resonant frequency (d) Main effect plot on resonant frequency

5.2. Different size cantilevers

Cantilever stiffness and piezoelectric surface area will effect cantilever performance, hence different size cantilevers are tested that can reflect the extent of influence of these factors.The factorial analysis data shows that size of cantilever does have an effect on resonant frequency and voltage output. Hence to get a deeper understanding of these effects and also to understand the impact it can have on internal resistance and power output, five sizes of commercial cantilevers are investigated (fig 24). The cantilever dimensions are given in table 7.

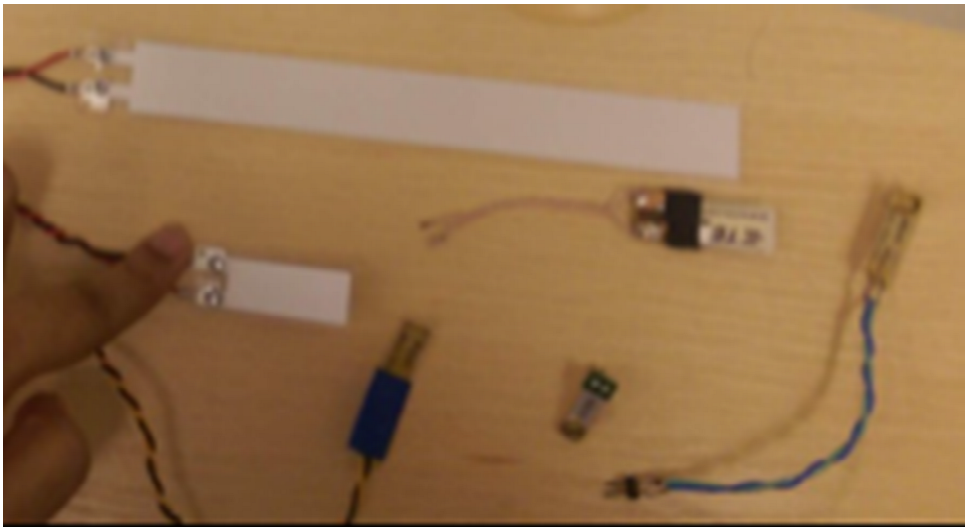

Fig 24. Photo of different size PVDF cantilevers used

With the same experiment set up shown in Fig. 17, PEC mounted on base actuator was excited with a pulse voltage of 1 V peak to peak V_{CV}, varying input frequencies between 10 Hz to 60 Hz, the open circuit output voltage was monitored.

Input pulse signals were provided at resonance frequency and voltage output was measured. The internal resistance of all cantilevers were calculated using equation (18) shown in table 7. Theoretical power for all cantilevers was calculated using equation (23). A comparison of resonant frequency, internal resistance and generated energy of different size cantilevers is given in table 7.

Table 7. Performance comparison of different size PE cantilevers

Dimensions(mm^3)	Vol(mm^3)	Acc(g)	$f_{res}(Hz)$	$R_i(M\Omega)$	E(μJ).
9.8×5.2× 0.205	10.4468	1	79.2	9.5	2.46
25× 13 × 0.205	66.625	1	62.8	4.5	13.65
41× 16 × 0.205	134.48	1	50.3	2	54.72
73× 16 × 0.205	239.44	1	44.2	0.8	24.81
171× 22 × 0.205	771.21	1	15.7	0.1	5.56

- **Effect of cantilever size on output**

Better stiffness of cantilever and more piezoelectric material both contribute to piezoelectric transduction. The shortest cantilever has more stiffness but less PE material. The largest cantilever in this comparison has low stiffness but more PE volume. It can observed that energy generated by the shortest and the largest cantilever is short compared to the medium sized cantilevers. This implies that the optimal size should be a trade off between volume and stiffness of cantilever. This idea is also reflected in the performance of the medium size cantilever having volume 134 mm^3, it produced 54.72 μJ energy outperforming the other PECs, the plot of output verses piezoelectric volume is shown in Fig. 25

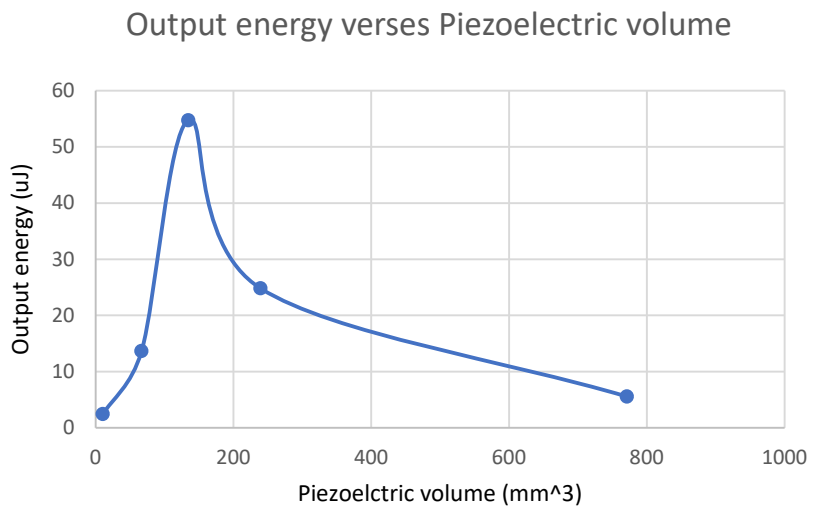

Fig 25. Plot of output verses piezoelectric volume

- **Effect of cantilever size on internal resistance**

It is observed that internal resistance decreases as PEC size increases. It is found that R_i is 9.5 $M\Omega$ for shortest cantilever and 0.1 $M\Omega$ for longest cantilever, this comparison is shown in Fig.26. For maximum energy to be generated, the optimal load resistance should be close to the internal resistance of the cantilever. The formula for optimal load resistance is [52],

$$R_{opt} = \frac{t}{WL\varepsilon_{33}\omega} = \frac{1}{C_p\omega} \qquad (31)$$

where, t is the thickness, L the length of PE layer, W the beam width, ε_{33} the dielectric constant, ω the angular frequency and C_p the parasitic capacitance of the PE material. This implies that optimal resistance varies with geometrical configurations and material properties. In this case, the material properties are same throughout, only the geometry of the cantilever changes. Since the cantilever thickness is same, only the length and width are contributing to the change in the resistance value.

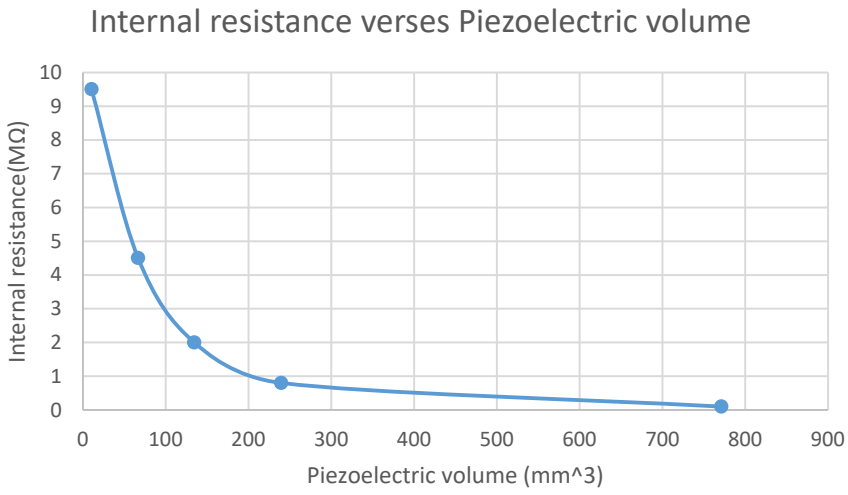

Fig 26. Plot of internal resistance verses piezoelectric volume

- **Effect of cantilever size on resonant frequency**

There is decrease in resonant frequency with increase in cantilever size. The frequency of resonance for the shortest cantilever is 79.2 Hz and 15.7 Hz for the longest cantilever. The plot below shows the effect of piezoelectric volume on resonant frequency, in Fig. 27

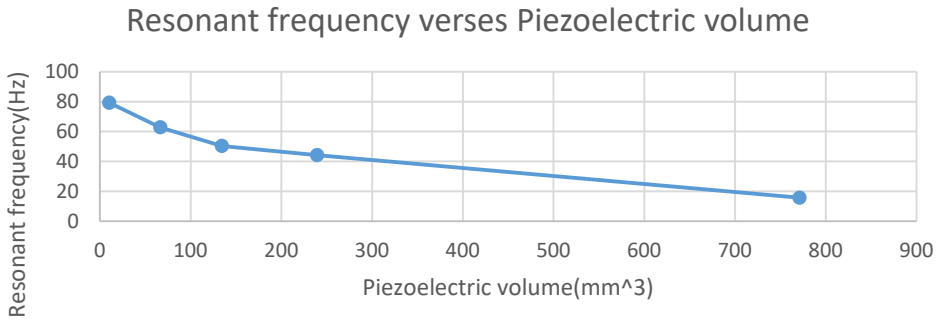

Fig 27. Plot of resonant frequency verses piezoelectric volume

5.3. Parallel arrangement of PE

In series configuration there is addition of individual voltages of ech PE layer whereas in parallel configuration there is addition of current generated in each layer [53]. With the intention to replicate the effect of parallel configuration, four commercial cantilevers are connected in parallel. The PECs are placed beside each other such that all the positive electrodes are connected together and all negative electrodes are connected together so that a single array is made. This section will show that combining four commercial PE cantilevers into a single array can improve effectiveness of the overall energy conversion across a wideband frequency spectrum over the case of a singleconverter.

Fig 28. The photo of experimental setup for PE array

- **Frequency response**

Fig. 28 gives the experimental setup used to find frequency response. Sinusoidal signal is the excitation applied with input frequency ranging from 30-70 Hz. Optimal load resistance of 2MΩ was used, tipmass of 2gm was fixed on the PE array free end. The frequency response for 3 acceleration levels is shown in Fig.29. For all the 3 levels of excitation 0.2g, 1g and 3g the resonant frequency of 47.5 Hz is observed. Fig 29 implies that the parallel array of PECs show non-linear behaviour. The advantage of non-linearity is that as compared to their liner counterparts, non-linear energy harvesters demonstrate improved performance under broadband excitation as well as longer device operation lifetime. However frequency tuning of a PEC is achievable either by changing the effective mass of the beam or its stiffness, by changing cantilever geometry or material properties. [54].

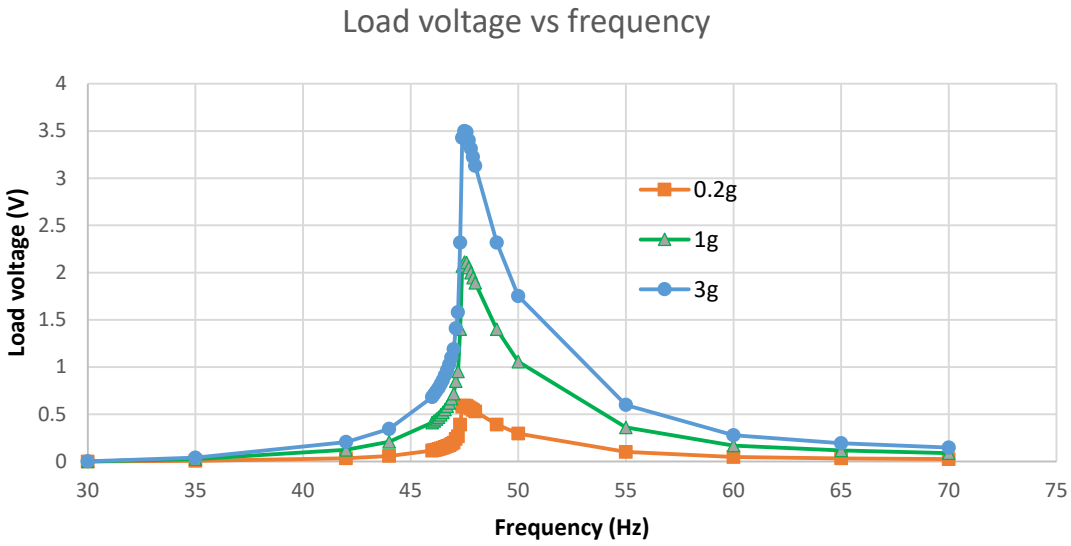

Fig 29. Frequency response of parallel array under excitations 0.2g, 1g and 3g

- **Voltage response and optimal load impedence**

This experiment was performed to understand how variation in load impedence effects the voltage and power generated. Table 8 and fig 30 show the load voltage and the power delivered to the load for different values of load resistance. In Fig. 30, the output voltage and power as a function of the resistive load is shown for three values of acceleration:0.2g, 1g and 3g. The simple relation, P=$V^2/2R$ was used to form this plot.

The plot in fig 30(a) implies that load voltage increases with an increase in load resistance, in this case up to approximately 7 V at 10 MΩ for 3g acceleration. A maximum power output of ~3.5 μW with 3.74 V DC voltage was obtained for the 2 MΩ load, at a resonant frequency of 47.5Hz, after which the electrical power gragually reduced with increase in load resistance, seen in fig 30(b).
Due to decrease in generated current with load resistance, the power delivered is maximized at the optimum load resistance. Hence, the power generated is higher at resonance and at a specific optimum load resistance. Thus, for this PEC array, the power density is 13.13 μW/cm^3 at 2MΩ optimal load resistance and resonant frequency 47.5 Hz.

Table 8. Voltage response for varying load resistance under different excitations

$f_{res}(Hz)$	$R_L(M\Omega)$	$V_{0.2g}(V)$	$P_{0.2g}(\mu W)$	$V_{1g}(V)$	$P_{1g}(\mu W)$	$V_{3g}(V)$	$P_{3g}(\mu W)$
46	0.1	0.06	0.02	0.30	0.45	0.50	1.25
48	0.47	0.25	0.06	0.97	1.00	1.58	2.66
47.6	0.68	0.35	0.09	1.13	0.94	1.93	2.74
47	0.82	0.40	0.10	1.30	1.03	2.12	2.74
47.4	1	0.46	0.11	1.50	1.13	2.53	3.21
47.6	1.5	0.55	0.10	1.96	1.28	3.19	3.39
47.5	2	0.62	0.10	2.26	1.28	3.74	3.50
48	5.6	0.95	0.08	3.39	1.03	5.80	3.00
49	10	1.18	0.07	4.06	0.82	6.94	2.41

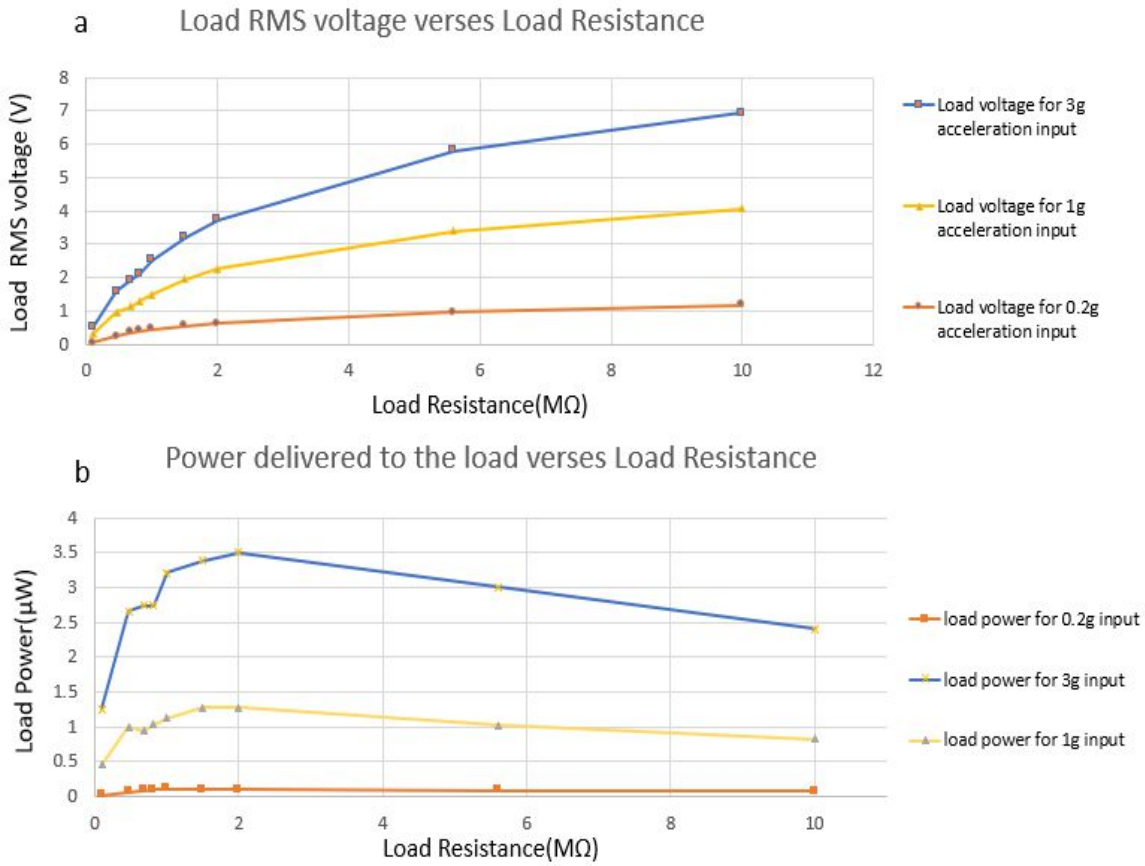

Fig 30. (a) Load rms voltage verses load resistance (b)Power delivered to load verses load resistance

- **Optimal tipmass and Gap**

Tipmass refers to the proof mass fixed to the free end of the cantilever and gap is the distance between tipmass and the fixed end of the cantilever. In order to research the effects of tipmass and gaps, four kinds of masses and three measures of gaps are used. To be comparable, mass and gap are kept stable in each experiment, respectively. The results obtained for these nine experiments, readings of load voltage as a function of tipmass and gap under excitation 0.2g to 3g are shown in table below.

Table 9. Load voltage as a function of tipmass and gap under excitation 0.2g to 3g

tipmass(gm)	0.9			1.8			2.3		
Gap (cm) →	0.6	0.8	1	0.6	0.8	1	0.6	0.8	1
$f_{res}(Hz)$ →	82	67.5	60.8	54	47.5	43.3	51	43	41.5
Input acc (g)	Load voltage (V)								
0.2	0.20	0.31	0.23	0.26	0.35	0.51	0.29	0.17	0.16
0.5	0.60	0.81	0.58	0.59	1.17	0.94	0.71	0.35	0.29
0.8	0.97	1.20	0.84	0.89	1.68	1.30	1.00	0.41	0.41
1.2	1.34	1.66	1.17	1.62	2.12	1.59	1.32	0.56	0.63
1.8	1.90	2.21	1.52	2.20	2.72	2.12	1.77	0.94	0.97
2.5	2.37	2.72	1.91	2.96	3.33	2.58	2.31	1.51	1.40
3	2.66	3.05	2.15	3.45	3.84	2.95	2.66	2.27	1.66

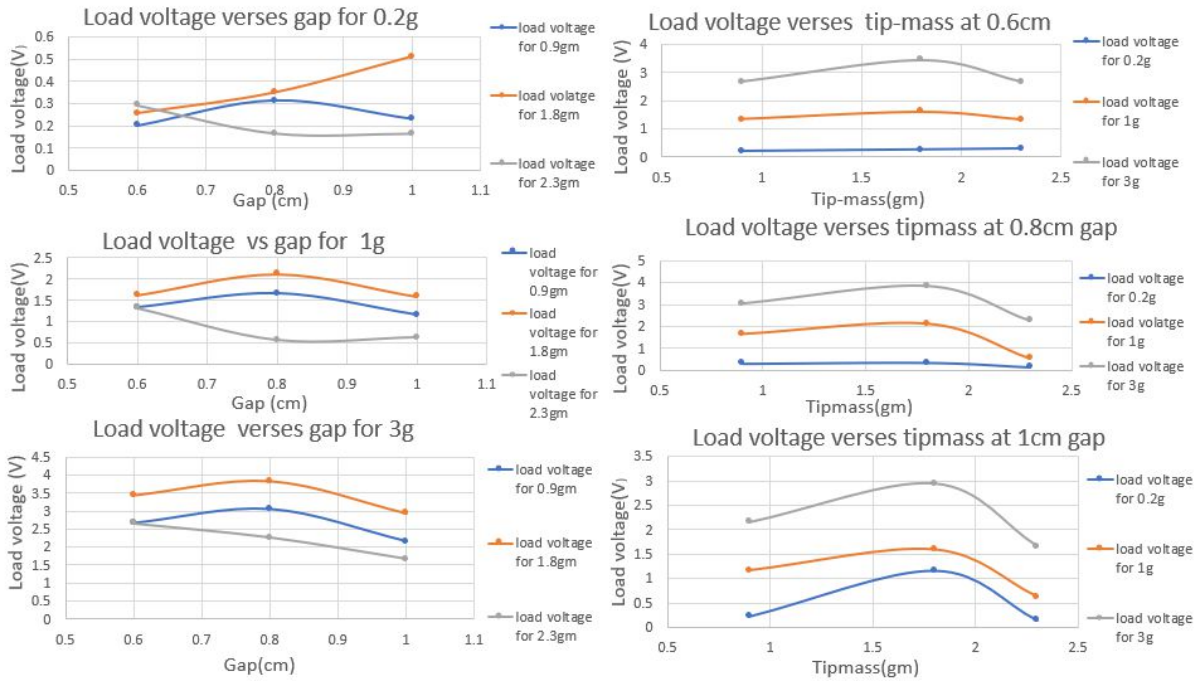

Fig 31. (a) Load voltage as a function of gap for 0.2g, 1g and 3g (b) Load voltage as a function of tipmass at gaps 6mm,8mm and 10mm.

The voltage produced is largest when the tipmass is impacted farthest to the clamped-end of the cantilever, and is lowest when the tipmass location is close to the clamped end. This is because, larger strain is produced when tipmass impacted locations farthest from the clamped end and hence more energy is converted. However in this experiment seen in Fig. 31(a) the optimal gap is found at 8mm from fixed end. In Fig. 31(b), tipmass 1.8gms imparts better results than the other weights used in this comparison. This tipmass and gap optimization is developed and adopted in the proposed PVEH design.

6. Proposed PVDF energy harvester

In the previous section, the output optimization was highest in the parallel array configuration. As it is already seen that stress developed in a cantilever during bending is maximum at the clamped end and decreases in magnitude away near the free end, hence to maximise this effect, the proposed harvester is made to have a longer width compared to its length so that the longer side can be clamped as seen in fig 32. Also, after analysing the performance of asymmetric commercial PECs, the fabricated harvesters are assured to have proper symmetry on either side of the neutral axis so that there is maximum bending and least damping.

The proposed PVEH consists of a base of passive material (e.g. steel) with active layers of piezoelectric material attached to it by conductive electrodes as shown in Fig. 32. The mechanical effects of the electrodes on the system are not important due to their extremely small thickness compared to the overall thickness of the transducer. It is assumed that the substrate and the layer of piezoelectric material are perfectly coupled, and that the electrodes are ideally conductive and exposed to the same difference of electrical potential. The PVDF film used is 30 μm thick, with a thin Al electrode on the surface, bonded in the same polling and stretching directions having a symmetric multilayer configuration as shown in fig 33(a). The geometric dimensions of the harvester and main parameters of PVDF are shown in Table 10 and Table 11, respectively. Structural steel was chosen as both the metal substrate and proof mass.

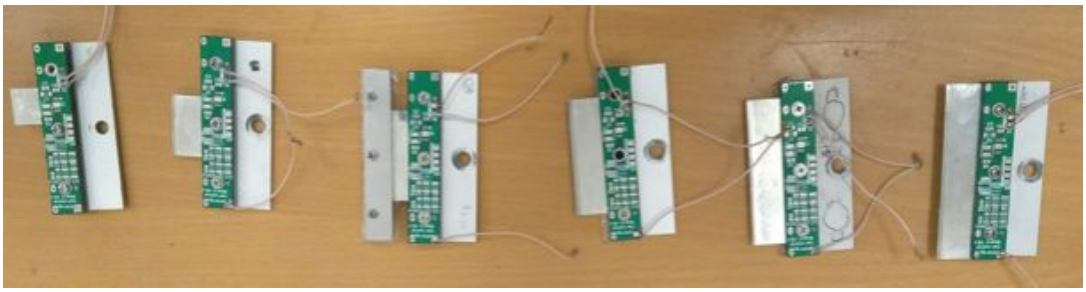

Fig 32. Harvester prototypes of width 14mm, 24mm, 34mm,44mm, 54mm and 64mm.

Table 10. Geometric values of the energy harvester model

Parameters	Symbols	Values
Dimensions of fixed end (mm)	$L_m \times W_m \times t_m$	$3\times 3 \times 3$
Dimensions of PVDF film(mm)	$L_e \times W_b \times t_b$	$14\times (24-64) \times 0.03$
Dimensions of steel (mm)	$L_e \times W_b \times t_s$	$23 \times (24-64) \times 0.01$
Dimensions of proof mass(mm)	$L_m \times W_m \times t_m$	$14\times (24-64)$
Weight of mass(g)	M	15-30
Gaps(mm)	L	5-10

Table 11. Parameters of energy harvester material

Piezoelectric material: PVDF (JINZHOUKEXIN Co. Ltd)		
Piezoelectric constant (pC/N)	d_{31}	25
Young's modulus (MPa/psi)	E	2500
Relative permittivity	$\varepsilon/\varepsilon_0$	9.5
Density(kg/m^3)	ρ_b	1780
Thickness(μm)	t_b	30

6.1. Fabrication process

A Simple constituent structure of the harvester is shown in Fig. 33(a). The PVDF and the metal substrate are cut in the dimensions given in table 10. The poling direction and the polarity of the PVDF should be kept in mind while gluing the PVDF to the substrate.The easiest way to check the poling direction is to stick a small piece of PVDF on the metal substrate using a temporal sticky substance like oil. Mark the poling direction at the clamped end of the PVDF. Excite the cantilever for a random signal and note down the open circuit voltage. Then rotate the PVDF by 90^0 i.e perpendicular to the previous direction marked and note down the open circuit voltage again. The case when higher voltage value is observed gives the poling direction.

In this study d_{31} piezoelectric coefficient is used which is commonly preferred in PVDF material. If more than one layer of piezoelectric material is used on either side of the cantilever then the polarity of the piezoelectric films should be taken care of. The positive and negative polarity of two PVDF films should never be stuck together, then the piezoelectric effect will be zero. Hence the poling direction and the polarity of the PVDF should be kept in mind while gluing the PVDF to the substrate. Fig. 33(b) shows the polarity and terminal combinations of multiple PVDF layers

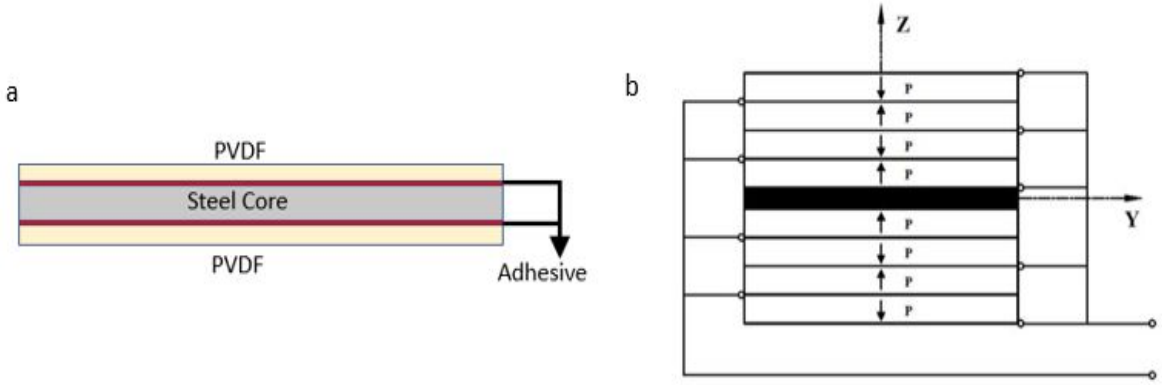

Fig 33. (a) Simple constituent structure of the harvester. (b) Polarization directions and terminal combinations for multilayer harvester [3]

6.2. Conductive adhesive

Epoxy resin is used as the gluing agent between PVDF layer and metal substrate. Compatibility and aging tests were performed to test the suitability of the adhesive. It is important to realise the effectiveness of the adhesive used as it should neatly paste the PVDF film to the metal base such that it looks like a single layer of material. Therefore to test the quality of the adhesive, aluminium foil was glued to the metal substrate using a very thin layer of epoxy resin and once the glue was dry the foil was divided into blocks as seen in Fig. 34. The resistance of each block is noted down before and after a long excitation is applied. The test is repeated every alternative day to discern the aging effect of the adhesive. Graphite power is also mixed with the adhesive for one of the samples, however it showed no effect on the resistance measured. Many samples were tested and the resistance readings of one of the samples is shown in table 12. The resistance measured was more or less consistent in all samples implying that the glue was intact and connected the foil to the metal base strongly. Different proportions of epoxy and hardener were applied and tested to find the optimum proportion of the two mixtures. It was found that equal proportions of epoxy and hardener form the right consistency in the glue mixture such that it is convenient to apply immediately within 20 minutes of

exposure to open air, before the mixture becomes too hard and this proportion also gives a strong and long lasting bonding between the PVDF layer and the metal substrate.

Fig 34. The aluminum foil cantilevers used to measure quality of glue

Table 12. Resistance of the aluminum(Al) foil glued on the metal base over a time period

Al part	day 1	2nd week	3rd week	4th week
	Resistance (Ω)			
1	1.7	2.2	1	1.4
2	3.2	4.8	0.7	0.9
3	25.3	26.1	26.8	62.4
4	2.3	2.8	1.3	1
5	2.7	3.7	16	18.6
6	1	2.2	1.1	1.6
7	7	8.4	0.6	0.9
8	1	2	1.5	1.4
9	0.9	2.5	0.6	1.1
10	2.1	4.4	3.6	2.2
11	2	3.1	1	1.5
12	1.6	2	1.6	2.7
13	1.1	2.9	1.2	3.5
14	1.8	2.6	1.3	2
15	7.4	8.9	21.6	25.4
16	9.5	10.7	0.6	1

6.3. Simulation and experimental analysis

The proposed harvester is modelled, simulated.and experimented. The influence of energy harvester excitation signal, energy harvester geometric configurations and shape variations, piezoelectric material layer thickness, connected electrical circuit resistance on energy harvester dynamic and electrical response was evaluated using the developed piezoelectric FEM model and experimental data.

- **Device model**

The PVEH is subjected to a selected kinematic excitation, which is described as a vertical or volumetric displacement of a volumetric load. Therefore, PVEH is excited, the active piezo layers generate a voltage signal. As shown in Fig. 17, signal generator outputs a specific frequency signal, after amplification the signal is used to excite the actuator to vibrate. The cantilever is fixed on the actuator. Oscilloscope and multimeter are used to measure peak-to-peak value and load rms value of the output voltage, respectively. Table 10 shows main parameters which were used for global definitions in COMSOL Multiphysics simulation software. The virtual interface between the piezoelectric power converter and the external electrical circuit was realized using SPICE electrical circuit simulation subroutine, in which the resistor was inserted as a variable (i.e., a variable impedance element) into the FEM model of the converter. A complex model of a vibrating electric converter is constructed, which evaluates the mutual electromechanical interaction between the piezoelectric converter and the connected electrical circuit.

In accordance to the design parameters in table 11, COMSOL Multiphysics software is used to build 2D finite element model (FEM) of a vibratory piezoelectric power converter, as shown in Fig.35. Solid mechanics, electrostatics and electrical circuits are used in numerical studies along with frequency domain study in COMSOL Multiphysics. The described FEM model (Fig.35) allows a complex evaluation of the transducer response, the electromechanical interaction of the energy harvester with the external electrical circuit, and the effects of nonlinear dynamics occurring in the vibrating mode of the harvester. The influence of energy harvester excitation signal, energy harvester geometric configurations and shape variations, piezoelectric material layer thickness, connected electrical circuit resistance on energy harvester dynamic and electrical response was evaluated using the developed piezoelectric FEM model.

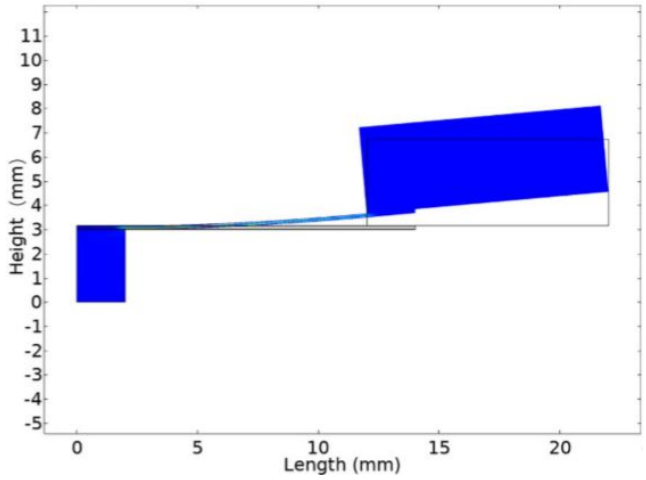

Fig 35. COMSOL finite models of PEH cantilever.

The results obtained when modelling a multilayer PEH using only the loss factor η are compared to the results obtained using the Rayleigh damping coefficient (Fig.36). In most publications on the modelling of piezoelectric transducers, frequency data and modelling results are provided using only the loss factor [55],[56]. The loss factor compares the damping of one material to another and it is does not depend on the geometrical parameters of the structure as it only relies on the material, but the geometrical parameters of the beam do affect damping and the output voltage. As seen in Fig.35,

the result of output voltage using loss factor is 50 % higher than real result, which is a theoretical value instead of a practical system value. Therefore, to evaluate the damping of the whole structure, Rayleigh damping is an effective way as it considers the damping of whole structure.

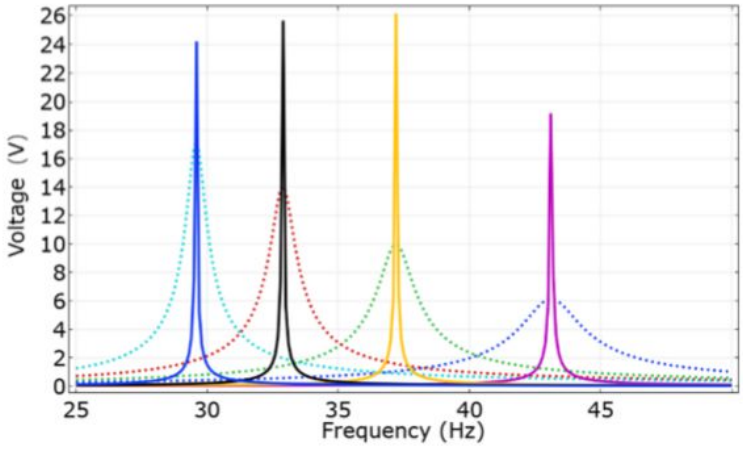

Fig 36. Voltage-frequency response of piezoelectric biomorph cantilever using loss factor

In fig 36, uniform line shows the results with the loss factor, the dotted line shows using the Rayleigh damping coefficient. To describe the FEM model, not only the material properties but also the damping ratio of the multilayer system is necessary to know. For this, experimental studies were carried out. Using the previous modelling results, the boundary conditions of the cantilever dimensions were obtained, from which the dependence of the system damping coefficient on the length, width and load mass of the cantilever was experimentally determined.

- **Damping ratio and Rayleigh dampling coefficents of the multilayer sytem**

Proportional or classical damping also known as Rayleigh's damping factor defines damping as a linear combination of the mass and stiffness matrices [57],

$$C = \alpha M + \beta k \qquad (32)$$

where M – mass matric, K – stiffness matric, α and β – real scalars with 1/s and s units respectively. Modes of classically damped systems preserve the simplicity of the real normal modes. To determine Rayleigh damping two specific frequencies ω1 and ω2 are used which is the value when half of maximum power is attained using optimal load resistance. Damping drastically increases and the modal responses at the corresponding frequency range are almost eliminated outside the range of frequencies ω1 and ω2. In fact, the high and low frequency vibrations/noises that are not within this range of frequency can be reduced with this method. The relations of Rayleigh damping coefficients α, β, damping ratio and two specific frequencies ω1 and ω2 are shown in equation (33)

$$\begin{bmatrix}\alpha \\ B\end{bmatrix} = \frac{2\zeta}{\omega_1+\omega_2}\begin{bmatrix}\omega_1\omega_2 \\ 1\end{bmatrix} \qquad (33)$$

Q factor describes an underdamped oscillator. One of the Q factor definitions is the frequency-to-bandwidth ratio of the resonator

$$Q=\frac{\omega_r}{\omega_2-\omega_1} \qquad (34)$$

where ωr is the resonant frequency, and ω2 – ω1 is the bandwidth, or the width of the range of frequencies for which the energy is half of its peak value. The relationship between Q factor and damping ratio is shown in equation (35)

$$\zeta = \frac{1}{2Q} \qquad (35)$$

In order to simulate the model, damping ratio and Rayleigh damping coefficients α and β are calculated. Five kinds of PVEHs with different widths of PVDF material are designed, ranging from 24 mm to 64 mm as shown in fig 32. According to the theoretical description of Rayleigh damping, the peak-to-peak value of output voltage under the resonant frequency is measured. Based on the peak-to-peak value, another two frequencies are measured where output power is half of the value measured under resonant frequency.

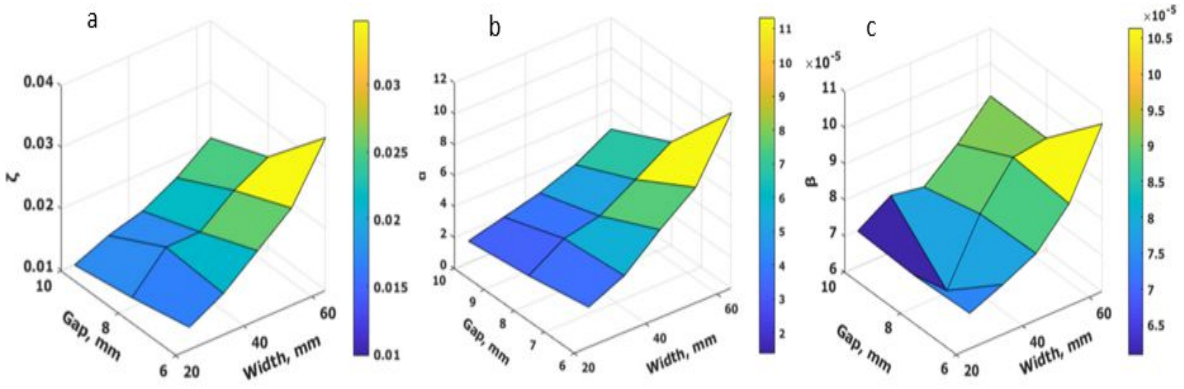

Fig 37. Results of damping coefficients: (a) damping ratio, (b) Rayleigh damping coefficient of α, (c) Rayleigh damping coefficient of β.

As shown in Fig 37, the result implies that the energy harvester is a linear vibration system. According to these data, damping coefficient of different gaps and widths can be approximately calculated using empirical approximation. C. Simulation Results using the dependence of the damping coefficient of the inverter on its length, width and load masses, FEM modelling was performed. The pulsed excitation signal is described in FEM model as a vertical load volume. The change of the effective voltage generated by the PE converter depending on the energy harvester parameters is recorded. Fig.40 gives the voltage as a function of the PVDF width under uniform load (15.2 g).

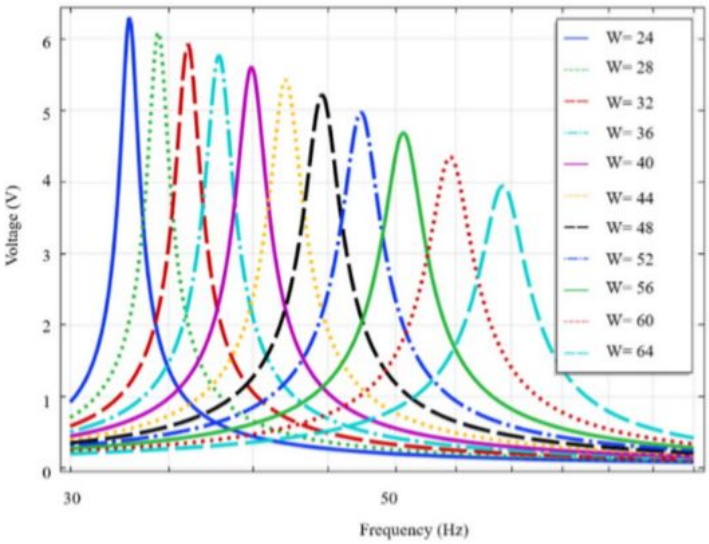

Fig 38 The voltage-frequency response of different width of PVDF

The dependence of the gap and the proof mass on output voltage of the structure are simulated. Optimal load resistance of 460 kΩ is selected. In order to research the effects of proof mass and gaps, simulated four kinds of masses and three kinds of gaps are simulated. To be comparable, mass and

gap are kept stable in each simulation, respectively. The voltage-frequency response curves of different masses are shown in Fig 39. It can be seen from these figures that by increasing the gap it is possible to obtain higher energy efficiency, but the resonant frequency decreases.

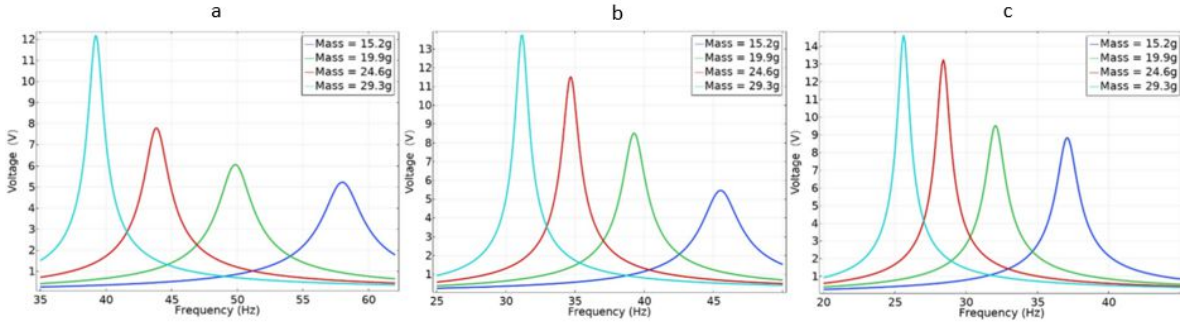

Fig 39. Simulation result of voltage-frequency response of different mass: (a) gap is 6 mm, (b) gap is 8 mm, (c) gap is 10 mm.

- **Experimental results and Discussion**

In order to crosscheck the simulation results, experiments were carried out. In Fig 40, the experimental voltage data of PVDF energy harvester cantilever is compared against the simulated voltage data at resonant frequency. As seen in Fig.40, the system's oscillation is identical to the typical response characteristics of linear vibration systems. The value of simulated voltage and measured voltage are fitted well. The differences of resonant frequency between simulation and measurement are no more than 4 Hz. It can also be seen in these three figures, that with the mass increasing, the output voltage increases in both simulation and experimental data.

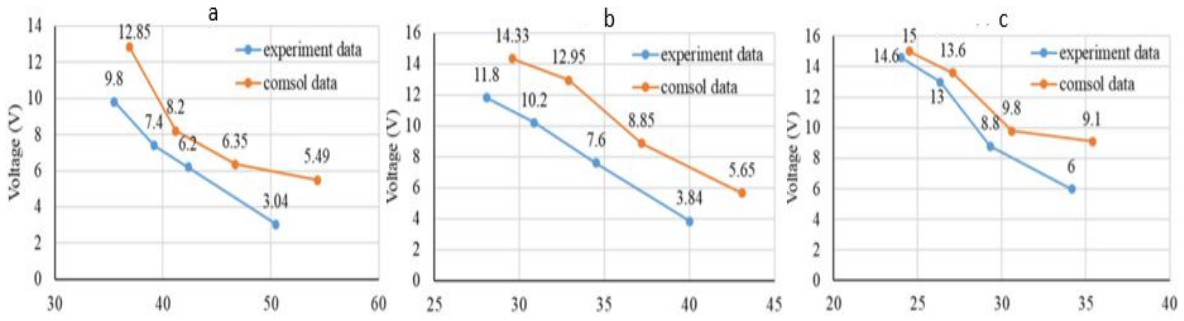

Fig 40 Experimental and simulated voltage data with different masses: (a) gap is 6 mm, (b) gap is 8 mm, (c) gap is 10 mm.

To identify how the gaps affect the output voltage, the output value of different gaps are compared. The results reflect changes of output voltage with gaps. As the gap gets bigger, the output voltage increases. According to the experimental data, the output voltage measured with maximum gap and mass is about 5 times of the voltage measured with minimum gap and mass. Obviously, increasing proof mass and gap can improve the output voltage and decrease resonant frequency. Some additional experiments were conducted with harvesters having 4 PVDF layers, the results were definitely better with output reaching up to 2 times that of a two layer harvester. However, the complexity of wiring electrodes cannot be ignored when more layers are used. Another interesting result was seen when instead of 100μm steel base,a 80 μm base was used as the rigid support for the PVDF layers and the result was surprisingly high as much as double the previous output.

7. Temperature dependence tests

The sensitivity of PVDF film and its pyroelectric effect can change with temperature. It is empirical to understand how the piezoelectric material generates charge when subjected to heat. Multilayer PVEHs can be sensitive to the variations in temperature because of "bimaterial" effect between PVDF and steel as the thermal dilation coefficients of both the materials are different. Stress can be thermally induced in multilayer cantilevers because of the difference in the thermal expansion coefficients of adjacent layers, or because the materials are subjected to temperature changes during their manufacturing and subsequent use. Deflection Δz varies linearly with same difference in temperature(< 3°C) in accordance with the thermal coefficients of PVDF a_{PVDF} or/and that of steel a_{Steel} such that [74] :

$$\Delta z = 3(a_{PVDF} - a_{Steel})\left(\frac{c+1}{B}\right)\left(\frac{L^2}{t_s}\right)\Delta T \qquad (36)$$

$$c=\frac{t_{PVDF}}{t_{steel}},\ B=4+6c+4c^2+jc^3+\frac{1}{jc},\ j=\frac{E_{PVDF}}{E_{steel}} \qquad (37)$$

where t_{steel} is thickness of steel; t_{PVDF} thickness of PVDF layer; E_{steel} is Young‘s modulas of steel; E_{PVDF} is Young‘s modulas of PVDF layer. Sensitivity in temperature is reduced due to non linearity of the cantilever response in higher temperatures. The sensitivity S_T in resonant frequency is caused by two reasons: firstly because of sensitivity of Young‘s modulus of each material with the temperature, and secondly due to bi-material effect stretching the layers out given by[75]:

$$S_T = \frac{df}{f_0 dT} = \left(\frac{a}{2}\right) + \left(\frac{dE}{2EdT}\right), a = \frac{(a_{PVDF}\, a_{Steel})}{a_{PVDF} a_{Steel}} \qquad (38)$$

7.1.Temperature test setup

Experimental setup is shown in Fig 43. Measurements were performed in the [-30 °C; 60 °C] temperature range with a maximum rate of 3 °C / min.The range of the temperature chamber is −70 °C to 150 °C and the error is ±0.1 °C [77]. To measure the influence of temperature, the actuator mounted with the harvester is placed in a temperature chamber (fig 43) and the signal input and output measuring circuit was connected to the outside of the chamber where the room temperature was stable. In all temperature tests excitation of the actuator is maintained low at 0.2g.

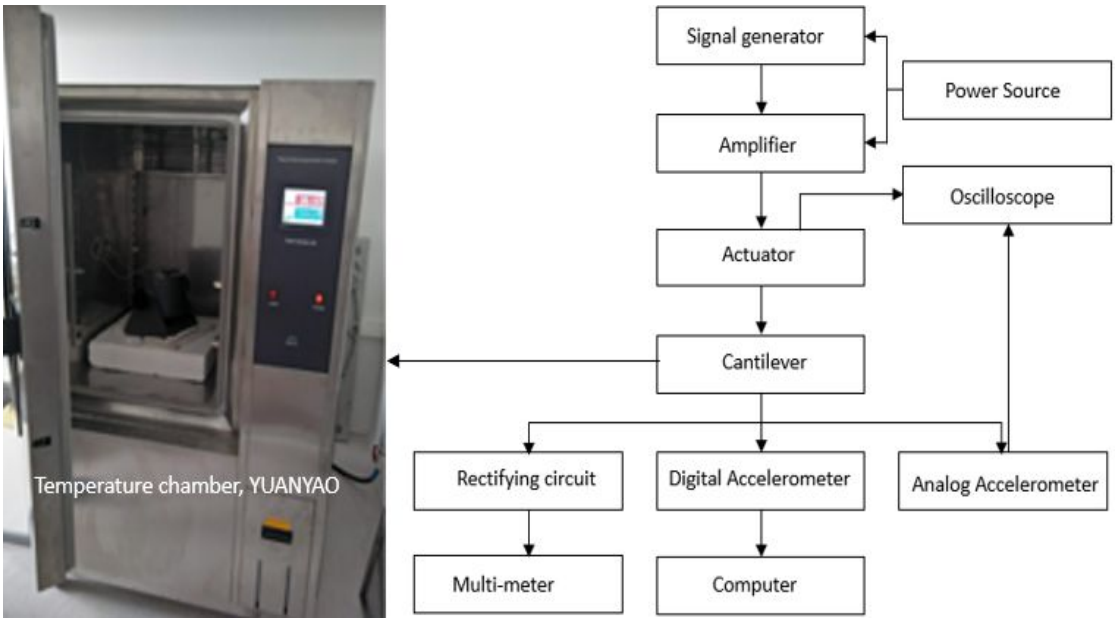

Fig 41. Flow chart of temperature test experiment setup

7.2. Shaker temperature test

Firstly only actuator is placed in the temperature chamber to observe the effect of the temperature change(-30^0C to $+60^0C$),a random signal with constant frequency of 45 Hz is used to excite the actuator and keeping constant acceleration of 0.2 g measured by the digital accelerometer, the actuator's coil excitation voltage V_{CV} is observed during the different temperatures set in the chamber

Table 13. Temperature chamber test results for actuator

T^0C	-30	-25	-20	-15	0	-5	0	5	10	15	20	25	30	35	40	45	50	55	60
mV	23	21	22	21	23	22	23	22	22	23	22	23	21	22	22	20	20	21	20

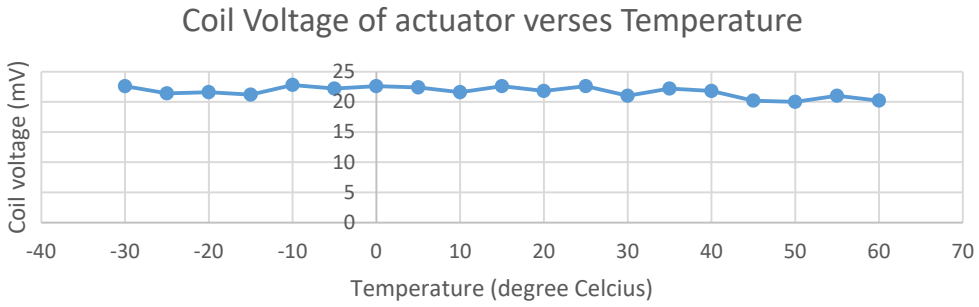

Fig 42. Temperature change effect on the coil excitation voltage requirement of actuator to maintain constant excitation 0.2g

It is obvious that the coil excitation volatge is lower in the positive temperatures than in the negative temperature region. It is also observed that between -30^0C and -10^0C the actuator behavior is abnormal, the input voltage is comparatively less to the coil excitation voltage in positive temperatures. Since this change is seen in the actuator, the same change can also be expected to reflect in the performance of the harvester when excited by this actuator in this temperature range.

7.3. Temperature test on parallel array of cantilevers

The parallel array of unimorph cantilevers discussed in section 5.3 was tested for temperature dependence. As mentioned in the previous subsection, temperature was varied from -30^0C to $+60^0C$. An optimal load resistance of 1.5 MΩ was used, maintaining constant acceleration of 0.2g,the values of V_{CV}, f_{res} and V_{rms} or load voltage were noted (table 14).

- The V_{CV} signal changes directly with increase in temperature and changes by +0.4V over the entire operating temperature range. This corresponds to a change of 0.004V / °C.(fig 43 (a))
- The V_{Rms} signal changes very little with increase in temperature and changes by +0.04V over the entire operating temperature range. This change is negligible and implies that plastic sensors without a steel core substrate have least dependence on temperature. (fig 43 (a))
- The f_{res} signal changes inversely with increase in temperature and changes by 8Hz over the entire operating temperature range. This corresponds to a change of 0.08Hz / °C.(fig 43 (b))

In the characterization of these cantilevers a clear dependence between resonance frequency and temperature is observed. However it is seen that the temperature change has very little effect on the rms voltage generated

Table 14. Temperature dependence of the parallel arrangement of 4 plastic sensors, under constant 0.2g excitation condition

T^0C	f_{res} (Hz)	V_{CV} (V)	V_{rms} (V)
-25	20.80	0.56	0.26
-20	20.50	0.57	0.14
-15	20.00	0.58	0.08
-10	19.00	0.62	0.19
-5	18.90	0.62	0.15
0	18.40	0.64	0.19
5	18.10	0.65	0.14
10	17.50	0.68	0.17
15	16.90	0.71	0.20
20	16.70	0.72	0.16
25	16.30	0.74	0.17
30	15.80	0.76	0.14
35	15.30	0.79	0.13
40	15.30	0.79	0.16
45	14.70	0.83	0.13
50	14.10	0.87	0.18
55	13.50	0.92	0.10
60	13.00	0.96	0.22

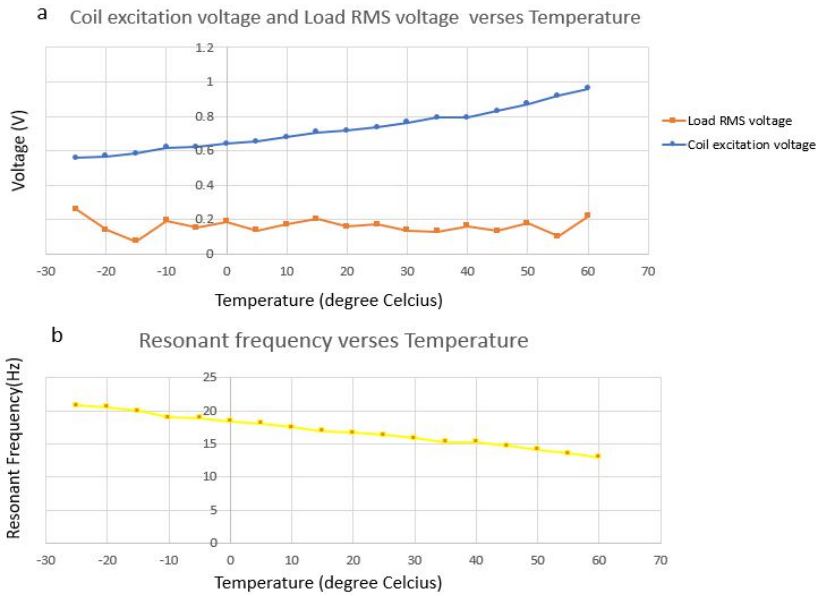

Fig 43. (a) Temperature change effect on the load rms voltage and coil excitation voltage of parallel array of commercial cantilevers at stable acceleration 0.2g.(b) Resoanant frequency verses temperature

7.4. Temperature test on fabricated harvester

The temperature response of energy harvester resonant frequency, coil excitation input requirement and output load rms voltage is evaluated for 6 fabricated harvester samples. The same procedure as discussed in the previous subsection is followed. Since this experiment is subjected to different harvester samples and each sample is individually tested in the temperature chamber, The average of the results considered is shown in table 15. This result is compared with the dependence of commercial cantilevers without rigid substrate. So this analysis will also give an idea as to whether the use of steel promotes the harvester performance during temperature change or limits its performance.

Table 15. Temperature dependence of the fabricated cantilever under constant 0.2g excitation condition

T^0C	f_{res} (Hz)	V_{CV} (V)	V_{Rms} (V)
-30	39.3	0.18	4.25
-25	39.3	0.18	4.10
-20	39.3	0.18	4.12
-15	39.4	0.17	4.23
-10	39.1	0.20	4.34
-5	39.4	0.21	5.15
0	39.4	0.22	5.32
5	39.6	0.23	5.67
10	39.5	0.23	5.72
15	39.3	0.23	5.72
20	39.3	0.24	5.74
25	39.4	0.24	5.66
30	39.3	0.24	6.02
35	39	0.24	5.61
40	39	0.25	5.85
45	39.1	0.25	6.21
50	39.1	0.25	6.43
55	39.1	0.25	6.69
60	38.8	0.29	7.22

- **Effect of Temperature on frequency**

Temperature change can show effects on resonant frequency which depends on material properties such as density and elasticity which are temperature dependent. Density of mass has some dependence on temperature due to thermal expansion with constant mass. Young's modulus of elasticity also shows a temperature dependence. These two effects show influence on resonant frequency [76]. As seen in plot of f_{res} verses temperature in fig 44, f_{res} decreases with increase in temperature at a rate of 0.005 Hz/°C and that of commercially available cantilevers is 0.08Hz / °C.It implies that the harvester resonant frequency has very less dependence on temperature.

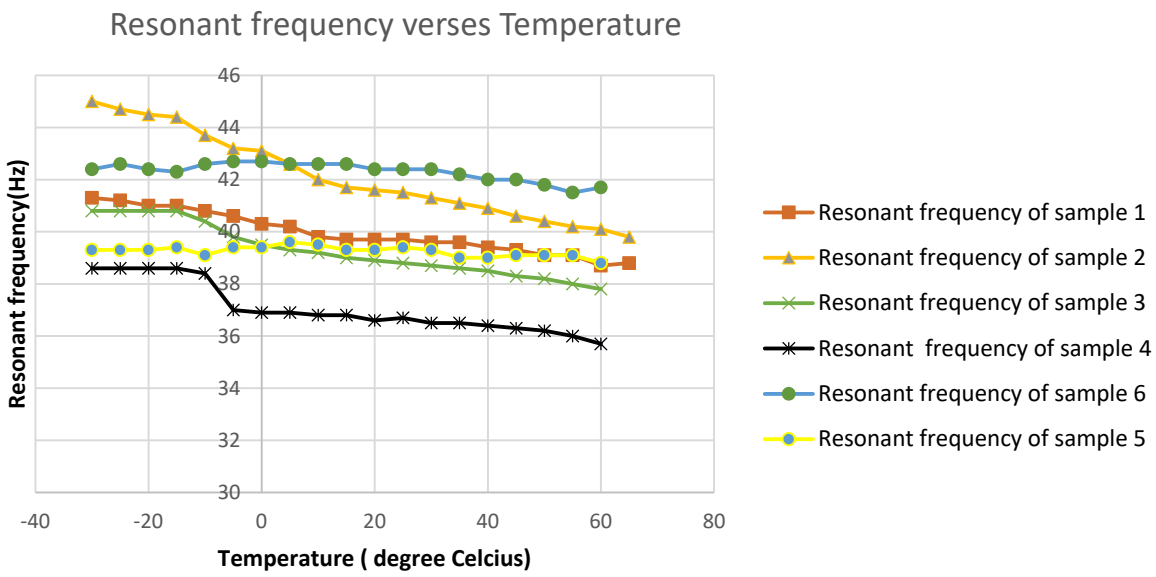

Fig 44. Temperature change effect on resonant frequency of fabricated PVEH at stable acceleration 0.2g.

- **Effect of Temperature on input coil excitation voltage of actuator**

The V_{CV} signal changes directly with increase in temperature and changes by +0.11V over the entire operating temperature range. This corresponds to a change of 0.0012V / ℃. The coil excitation voltage requirement is increasing at this rate, which is much less compared to 0.004 V/℃ of commercial cantilevers. As seen in fig 45, the harvester comparatively needs less input voltage in lower temperatures than in higher temperatures.

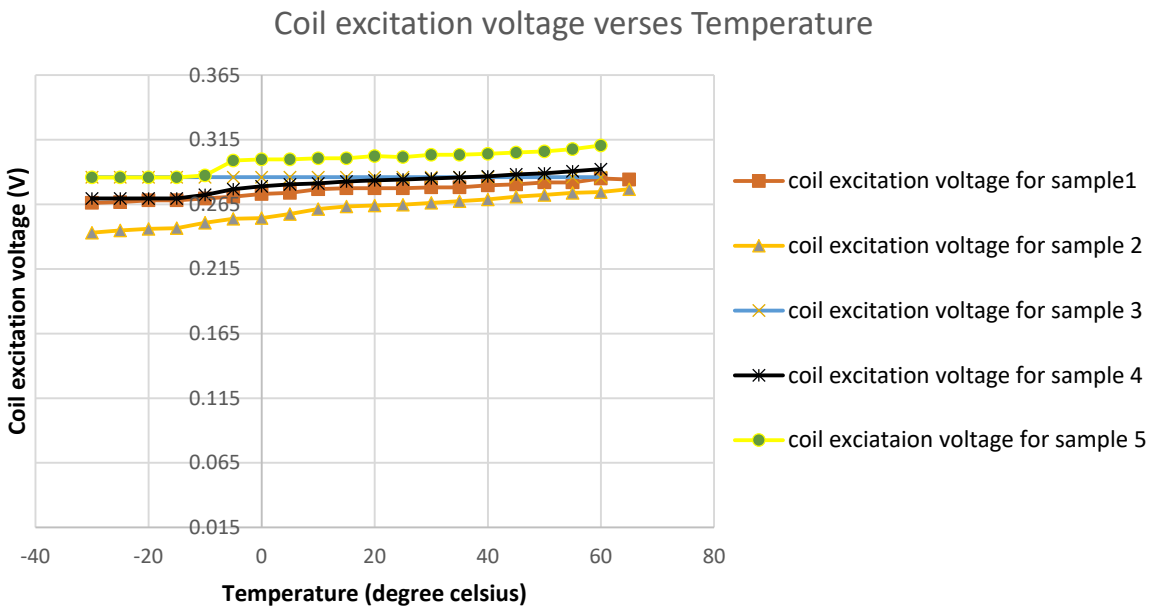

Fig 45. Influence of ambient temperature fluctuation on the coil excitation voltage at stable acceleration 0.2g.

- **Effect of temperature on output load rms voltage of Harvester**

The output V_{Rms} voltage increases directly with increase in temperature and changes by +3V over the entire operating temperature range. This corresponds to a change of 0.03V / ℃ which is similar to 0.04 V / ℃ of commercial cantilevers.However there is a drop of approximately 1 V in V_{Rms} value between -25℃ to -5℃ shown in fig 46. This is more likely the behavior of the actuator under negative temperature conditions as verified by the temperature dependence experiment conducted on the actuator

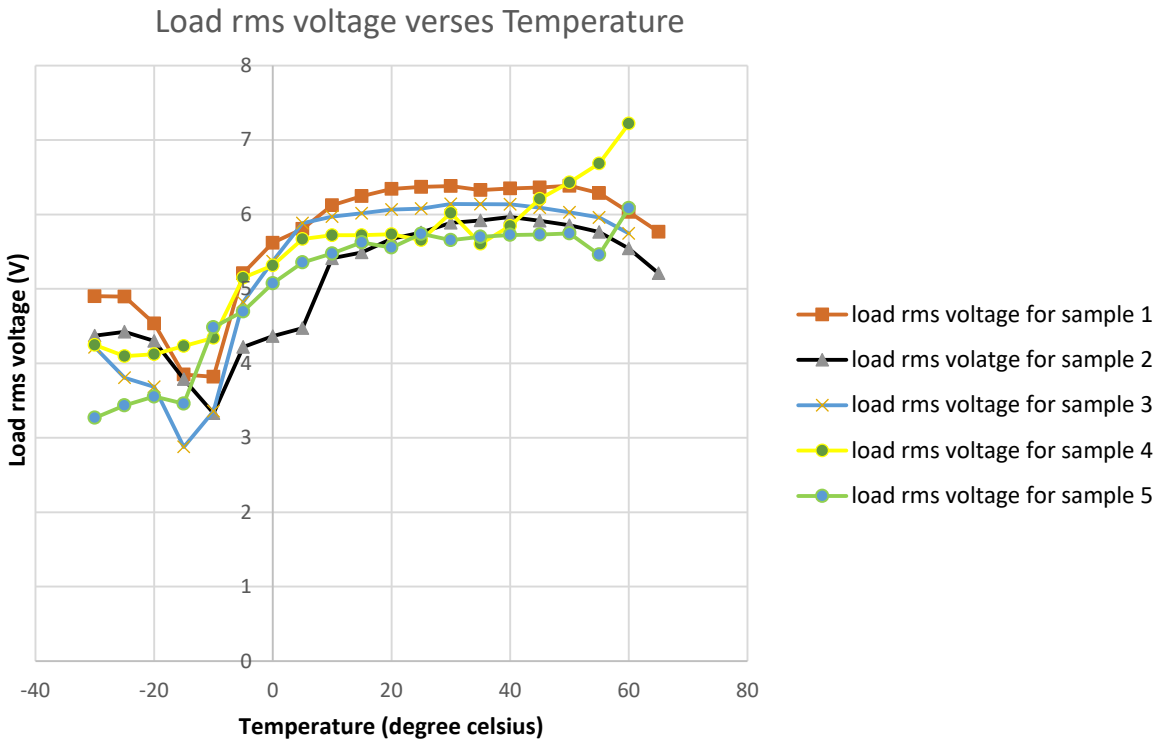

Fig 46. Temperature change effect on the output signal of the fabricated harvester at stable acceleration 0.2g.

8. Comparison of proposed harvester with other published works and future recommendations

PVEHs made of different piezoelectric materials are shown in table 16. Serial numbers 1 to 7 show PZT(Lead Zirconate Titanate) harvesters, 8 and 9 are of PMT-PT (Lead Mangesium Niobate-Lead TitanatePotassium), number 10 is made of KNN(Sodium Potassium Niobate), 11 is of AlN(Aluminium Nitrate) and the rest 12- to 20 comprise of PVDF(Polyvinylidene fluoride)layers.

Table 16. Comparison of proposed harvester with other material harvesters from other published works

Sl No	PE layer	ACC (g)	f_{res} (Hz)	P_{max} (μW)	$\left(\frac{P}{vol}\right), \left(\frac{mW}{cm^3}\right)$	$\frac{P/vol}{Acc}, \left(\frac{mW/cm^3}{g}\right)$	Ref
1	PZT	0.25	109.5	335.2	0.296	1.184	[58]
2	PZT	0.6	42	0.114	1.48	2.47	[59]
3	PZT	1	29.6	15300	13.5	13.5	[60]
4	PZT	0.4	20	1500	93.2	233	[61]
5	PZT	2	130	3000	125	62.5	[62]
6	PZT	2.5	344	2.5	12.5	5	[63]
7	PZT	1	89	15.4	3.62	3.62	[64]
8	PMN-PT	2	237	5.93	9.83	4.92	[65]
9	PMN-PT	0.23	174	586	0.753	3.27	[66]
10	KNN	1	132	3.62	1.8	1.8	[67]
11	AIN	1.6	69	8.7	5.18	3.23	[68]
12	PVDF	1.7	55	4.3	0.65	0.38	[69]
13	PVDF	0.5	34.4	112.8	8.61	17.22	[70]
14	PVDF	1.2	17	16	0.176	0.15	[71]
15	PVDF	1	103.8	10.6	1.94	1.94	[72]
16	PVDF	0.5	30	4.5	0.058	0.116	[73]
17	PVDF	0.8	33	0.9	0.028	0.035	[51]
18	PVDF	0.5	30.8	8.59	0.110	0.220	[3]
19	PVDF	3	47.5	3.5	13.13	4.37	Array PECs
20	PVDF	0.4	26	435	8.092	20.229	this work PVEH

Table 17. Comparison of PZT, PMT-PT and PVDF material properties [78],[79]

Property	PZT	PMT-PT	PVDF
Strain coefficient(d_{31}), 10^{-12}m/v	320	420	25
Strain coefficient(d_{33}), 10^{-12}m/v	650	850	30
Coupling coefficient(k_{31}), CV/Nm	0.44	0.65	0.11
Coupling coefficient(k_{33}), CV/Nm	0.75	0.88	0.16
Dielectric Constant,$\varepsilon\ /\ \varepsilon_0$	3800	3760	9.5
Elastic modulus, $10^{10}N/m^2$	5	0.83	0.3
Tensile strength, $10^{10}N/m^2$	2	8.3	5.2

Reviewing information presented in both tables 16 and17, one may conclude that,

- PZT having high material properties is widely used, yet brittle, which causes limitations in strain level that can be applied for energy harvester. Although PMN-PT is demonstrating great PE properties, it is even more brittle than PZT and, moreover, highly expensive, thus not very suitable for vast practical applications.
- PVDF is capable of handling large strain, allows mechanical energy available for conversion into electrical energy, despite its low electromechanical coupling coefficient it is in demand because of its higher tensile strength, lower stiffness and its ease of integration in manufacturing processes.
- The real PVDF energy harvester proposed in this thesis has a power density of 20. 23 $\mathrm{mW/cm^3}$ /g, generating at least $14V_{RMS}$ voltage and 435 μW power for optimal load impedance of 460kΩ being subjected to an acceleration of 0.4g.(table 16 number 20), which is the highest power density achievable for PVDF based harvesters, in fact better than most PZT material harvesters.
- Also the parallel array of commercial cantilevers shown in section 5.3, prove to have power density of 4.37 $\mathrm{mW/cm^3}$ /g which is extraordinary for harvesters without any rigid substrate.

Future Recommendations

- Following results of performed literature review and conclusions that were drawn from PE materials' advantages/disadvantages, it can said that it was a right decision to choose PVDF as a primary material for simulations, prototyping and experimental research described in this thesis. Research should be conducted to find new kinds of piezoelectrets with higher PE coefficients, for example a porous polydimethylsiloxane (PDMS)-based piezoelectret was proposed to have d_{33} values upto ~1500 pC/N by Wang et al., [80]. Attempt has to be made to incorporate such materials in proposed kind of harvesters.
- With the same harvester design, more PE layers and/or thinner substate material could be used to increase the power generation.
- The harvested power of a PEC beam is affected by type of substrate surface. A sticky surface which causes the PE material to stick better on substrate could increase the power output, thus, a new design must consider having a stickier surface and yet avoid application of thick layer of adhesive on the substrate surface.
- As shown in the first chapter only β -phase of PVDF shows strong piezoelectricity, hence a dedicated study on the β -phase component of PVDF material can probably lead to increase in productivity of PVDF-based energy harvesters.
- A more important issue is the power generated per unit area,as illustrated in literature review, power output due to tipmass impact decreased from the open-end of the cantilever to the fix end, new type of harvesters could be designed in such a way that there is no fix-end(s).
- Effort on optimizing the circuit efficiency was only done on finding the optimum load resistance, but studies on interface circuits are still lacking. Therefore, extensive investigations should be made to test the suitability and efficiency for PE energy harvesters.
- Apart from searching for new piezo material that could have a high piezoelectric coefficient, the pre-biasing technique to enhance the damping force of the PE transducers proposed in [48] could also be a good choice.
- Apart from these, innovative methods should be developed to integrate more types of energy harvesters into one hybrid renewable energy system.

Conclusions

Conclusions are presented here chapterwise:

I. **Chapter 1**:This thesis has done a comprehensive literature review recognizing the problems in energy harvesting technology like low energy output, low voltage output, high amount of external components, large form factor on PCB, along with an overview of PEH fundamentals, basic configuration, bimorph, unimorph and multilayer cantilevers, PEC shapes, types of PE materials, importance of poling direction, PE coefficient, interfacing circuits, application of energy harvesting and few performance enhancement techniques are summarized.

II. **Chapter 2**:Theoretical analysis, factorial analysis, simple and easy to implement equations for internal resistance and maximum theoretical power estimation was performed and theoretical measurement accuracy was evaluated.

III. **Chapter 3** :Tests were performed on actuator and the following conclusions were drawn.

- The actuator was calibrated with respect to the input supply frequency, input coil excitation voltage (V_{CV}) and acceleration voltage (V_{AV}). The deviation between calculated acceleration value and actual acceleration measured is $\pm 1\%$, hence with proposed equation actuator acceleration value can be found knowing only the coil excitation voltage or the analog accelerometer voltage value. Therefore, relationship between measured acceleration, coil excitation voltage and analog accelerometer voltage is well established.
- Investigation of effect of weight on actuator performance made it clear that, mounted object weight had no significant effect on the actuator performance. However, at lower frequencies the actuator required more input to maintain constant acceleration.

IV. **Chapter 4** : The initial considerations of investigation gave the following conclusions.

- The pulse width of the input signal was adjusted to 10ms such that the cantilever and the actuator moved with maximum resonance.

V. The considered interfacing circuit is simple for practical implementation with only a maximum 0.6V voltage drop on the rectifer diode bridge. In this research work, such a system seems to be productive with regard to the attained frequency bandwidth and secured output power**.**

VI. **Chapter 5** :Investigation on commercial cantilevers imply the following conclusions.

- The factorial analyses using minitab showed that output obtained when the cantilever size is increased more than twice is equal to output obtained when twice heavier tipmass is used. This could possibly mean that rather than increasing the cantilever size one could add more tipmass to obtain better results.
- Investigation on different size commercial cantilevers convey the following.
  - **Effect of cantilever size on output-** The cantilever that produced maximum output had dimensions $41 \times 16 \times 0.205\ mm^3$, developed 54.72 µJ energy at 60.91% efficiency outperforming the other cantilevers, conveying that optimal size should be a trade off between piezoelectric volume and cantilever stiffness
  - **Effect of cantilever size on internal resistance-**The internal resistance decreases as cantilever size increases.
  - **Effect of cantilever size on resonant frequency** -Resonant frequency decreases with increases in cantilever size.

- From investigation on parallel array arragement the following conclusions are drawn.
  - It was observed that combining four commercial PE cantilevers into a single array magnified the effectiveness of the entire energy conversion across a wide range of frequency, proving to be better than a single converter.
  - **Frequency response-** Impied that the parallel array is non-linear, demonstrates improved performance under broadband excitation and also has longer device operation lifetime.
  - **Voltage response and estimation of optimal load impedence-** A maximum power output of ~3.5 μW with 3.74 V DC voltage was obtained for optimal load resistance 2 MΩ, at a resonant frequency of 47.5Hz, after which the electrical power decreased with an increase in load resistance. Thus, for parallel array PECs, the power density is 4.37 $\mathrm{mW/cm^3}$ /g .
  - Resonant frequency is constant for different load resistances applied.
  - **Estimation of Optimal tipmass and Gap-** the optimal gap is neither at the extreme end nor at the nearest end, it is found that a gap of 8mm from the fixed end results in maximum output and tipmass of 1.8gms produced better results than the other weights used in this comparison.

VII. **Chapter 6:** Fabrication, modelling and optimization can be summarized by the following conclusions.

- The quality test of conductive adhesive done to discern the aging effect reveals that the conductivity was consistent in all samples measured at different intervals of time, hence adhesive is reliable for long term use.
- Cantilever modeling using only the loss factor is too inaccurate for use in cantilever optimizing and does not give sufficient accurate results.
- A more accurate model and simulation was built in COMSOL Multiphysics simulation software based on the measurements of Rayleigh damping coefficients. The COMSOL simulation results resemble experiment data.
- Experimental determination of Rayleigh Damping Coefficients, linear approximation, and modeling of cantilever give results with sufficient error (up to 10 %).
- According to both experimental data and simulation data, increasing the gap and proof mass increases the output voltage. Under the conditions of 0.4 g acceleration, 10 mm gap and 29.3 grams proof mass, the output voltage can up to 14.6 V and power is 435 μW. Comparing with the smallest gap and proof mass, proper PEH optimization can increase a voltage output up to 5 times.

VIII. **Chapter 7** : To the best of our knowledge, the analysis presented in this section was performed for the very first time. Upon completion of series of measurements it is evident that the harvester temperature curve has given a sufficient detailed picture of the temperature-dependent effects and the conclusions are presented as follows.

- **Shaker temperature test**
  - The coil excitation voltage is comparatively lower in the positive temperatures than in the negative temperature region at stable acceleration.
  - It is also observed that between -30^0C and -10^0C the actuator behavior is abnormal, there is sudden drop in coil excitation voltage while maintaining constant acceleration of 0.2g.

- **Temperature test on parallel array of cantilevers.**
  - The V_{CV} signal changes directly with increase in temperature and changes by 0.4V over the entire operating temperature range. This corresponds to a change of 0.004V / ℃.
  - The V_{Rms} signal changes very little with increase in temperature and changes by 0.04V over the entire operating temperature range. This change is negligible and implies that plastic sensors without a steel core substrate have least dependence on temperature.
  - The f_{res} signal changes inversely with increase in temperature and changes by 8 Hz over the entire operating temperature range. This corresponds to a change of 0.08Hz / ℃.
  - In the characterization of these cantilevers a clear dependence between resonance frequency and temperature is observed. However it is seen that the temperature change has very little effect on the rms voltage generated.

- **Temperature test on fabricated harvester**
  - **Effect of Temperature on frequency-** f_{res} decreases with increase in temperature at a rate of 0.005 Hz/℃ and at 0.08Hz / ℃. for commercial cantilevers. It implies that the harvester resonant frequency has very less dependence on temperature.
  - **Effect of Temperature on input coil excitation voltage of actuator-** The V_{CV} signal changes directly with increase in temperature and changes by 0.11V over the entire operating temperature range. This corresponds to a change of 0.0012V / ℃. The coil excitation voltage requirement is increasing at this rate, which is much less compared to rate of 0.004 V/℃ of commercial cantilevers. The harvester comparatively needs less input voltage in lower temperatures than in higher temperatures
  - **Effect of temperature on output load rms voltage of Harvester-** The output V_{Rms} voltage increases directly with increase in temperature and changes by 3V over the entire operating temperature range. This corresponds to a change of 0.03V / ℃ which is similar to 0.04 V / ℃ of commercial cantilevers

IX. **Chapter 8** proved that proposed PVDF energy harvester is among the highest power generating harvesters till date and on par with PZT material energy harvesters, with power output of 20. 23 $\mathrm{mW/cm^3}$ /g.

- With such power generation capacity, the proposed harvester can have a number of applications. It can be installed in any machine engine having ambient vibration like in grass movers, chain saw machines etc.
- This result compared with other sources is very well justified by the extent of optimization, investigation and analysis shown in the previous chapters, proving to be a boon for weakly coupled low profile PE material like PVDF.
- Hence, despite the low PE coupling seen in PVDF its energy harvesting capability can be profusely increased using the proposed harvester piezoelectric beam configuration.
- The key problems and future research suggestions for development in this field are discussed.

References

[1] Milašauskaitė, Ieva. "Research of dynamics of piezoelectric energy harvesters." PhD diss., Kaunas University of Technology, 2014.

[2] Yang, Yaowen, and Lihua Tang. "Equivalent circuit modeling of piezoelectric energy harvesters." *Journal of intelligent material systems and structures* 20.18 (2009): 2223-2235.

[3] Rammohan, S., C. Sanketh, C. M. Ramya, S. Jayanth Kumar, Jain Anjana, and Pratap Rudra. "Multi-layer piezoelectric energy harvesters for improved power generation." (2014): 1-6.

[4] Liu, Huicong, Junwen Zhong, Chengkuo Lee, Seung-Wuk Lee, and Liwei Lin. "A comprehensive review on piezoelectric energy harvesting technology: Materials, mechanisms, and applications." *Applied Physics Reviews* 5, no. 4 (2018): 041306.

[5] Savanth, Anand, Alex S. Weddell, James Myers, David Flynn, and Bashir M. Al-Hashimi. "Integrated reciprocal conversion with selective direct operation for energy harvesting systems." IEEE Transactions on Circuits and Systems I: Regular Papers 64, no. 9 (2017): 2370-2379.

[6] "Nowi-energy "[interactive][last accessed on 2020-01-20] available at https://www.nowi-energy.com/

[7] Ramadass, Yogesh K., and Anantha P. Chandrakasan. "An efficient piezoelectric energy harvesting interface circuit using a bias-flip rectifier and shared inductor." *IEEE journal of solid-state circuits* 45, no. 1 (2009): 189-204.

[8] Kim, Woon Kyung. "Design and analysis of switching circuits for energy harvesting in piezostrutures." PhD diss., Virginia Tech, 2012.

[9] Chua, Kok Gnee, Yew Fong Hor, and Hee C. Lim. "Raindrop kinetic energy piezoelectric harvesters and relevant interface circuits: Review, issues and outlooks." *Sensors & transducers* 200, no. 5 (2016): 1.

[10] Lefeuvre, Elie, David Audigier, Claude Richard, and Daniel Guyomar. "Buck-boost converter for sensorless power optimization of piezoelectric energy harvester." *IEEE Transactions on Power Electronics* 22, no. 5 (2007): 2018-2025

[11] Lallart, Mickaël, and Daniel Guyomar. "An optimized self-powered switching circuit for non-linear energy harvesting with low voltage output." *Smart Materials and Structures* 17, no. 3 (2008): 035030.

[12] Elliott, A. D. T., and P. D. Mitcheson. "Power density improvement of a piezoelectric energy harvester through use of a micropower switch-mode interface." In *SENSORS, 2012 IEEE*, pp. 1-4. IEEE, 2012

[13] Dicken, James, Paul D. Mitcheson, Ivan Stoianov, and Eric M. Yeatman. "Increased power output from piezoelectric energy harvesters by pre-biasing." (2009)

[14] Bhasker, M. Udaya. "Piezoelectric Energy harvesting from shoes of Soldier." In *2016 IEEE 1st International Conference on Power Electronics, Intelligent Control and Energy Systems (ICPEICES)*, pp. 1-5. IEEE, 2016..

[15] Wang, Zhong Lin, Jun Chen, and Long Lin. "Progress in triboelectric nanogenerators as a new energy technology and self-powered sensors." *Energy & Environmental Science* 8, no. 8 (2015): 2250-2282

[16] Song, Yewon, Chan Ho Yang, Seong Kwang Hong, Sung Joo Hwang, Jeong Hun Kim, Ji Young Choi, Seung Ki Ryu, and Tae Hyun Sung. "Road energy harvester designed as a macro-power source using the piezoelectric effect." *International Journal of Hydrogen Energy* 41, no. 29 (2016): 12563-12568

[17] Ghosh, Sujoy Kumar, and Dipankar Mandal. "Efficient natural piezoelectric nanogenerator: electricity generation from fish swim bladder." *Nano Energy* 28 (2016): 356-365.
[18] Kaval, William G., Robert A. Lake, and Ronald A. Coutu. "PVDF-TrFE Electroactive Polymer Based Micro-Electro-Mechanical Systems (MEMs) Structures." In *Micro and Nanomechanics, Volume 5*, pp. 11-17. Springer, Cham, 2018.
[19] Tuukkanen, Sampo, and Satu Rajala. "A survey of printable piezoelectric sensors." In *2015 IEEE SENSORS*, pp. 1-4. IEEE, 2015.
[20] Han, Bing, Xiaohui Ning, Qingling Meng, Jin Yan, Chenchen Xie, Ran Ding, and Zuobin Wang. "High output piezoelectric composite nanogenerators composed of FAPbBr 3-PVDF." In *2017 IEEE International Conference on Manipulation, Manufacturing and Measurement on the Nanoscale (3M-NANO)*, pp. 371-374. IEEE, 2017.
[21] Eggborn, Timothy. "Analytical models to predict power harvesting with piezoelectric materials." PhD diss., Virginia Tech, 2003.
[22] Stroyan, Jared James. "Processing and characterization of PVDF, PVDF-TrFE, and PVDF-TrFE-PZT composites." (2004).
[23] Emad, Ahmed, Mohamed AE Mahmoud, Maged Ghoneima, and Mohamed Dessouky. "Modeling and analysis of stretching strain in clamped-clamped beams for energy harvesting." In *2016 IEEE 59th International Midwest Symposium on Circuits and Systems (MWSCAS)*, pp. 1-4. IEEE, 2016.
[24] Elliott, A. D. T., and P. D. Mitcheson. "Power density improvement of a piezoelectric energy harvester through use of a micropower switch-mode interface." In *SENSORS, 2012 IEEE*, pp. 1-4. IEEE, 2012.
[25] Zhu, Dibin, Ahmed Almusallam, Steve Beeby, John Tudor, and Nick Harris. "A bimorph multi-layer piezoelectric vibration energy harvester." (2010).
[26] Mateu, Loreto, and Francesc Moll. "Optimum piezoelectric bending beam structures for energy harvesting using shoe inserts." *Journal of Intelligent Material Systems and Structures* 16, no. 10 (2005): 835-845.
[27] Roundy, Shad. "On the effectiveness of vibration-based energy harvesting." *Journal of intelligent material systems and structures* 16, no. 10 (2005): 809-823.
[28] Baker, Jessy, Shad Roundy, and Paul Wright. "Alternative geometries for increasing power density in vibration energy scavenging for wireless sensor networks." In *3rd international energy conversion engineering conference*, p. 5617. 2005.
[29] D. Andriukaitis, R. Anilionis, "Investigation of Etching Process in Nano Structures," Elektronika ir elektrotechnika, vol. 86, no. 6, pp. 7780, 2008.
[30] Kumar, Tarun, Rajeev Kumar, and Vishal Singh Chauhan. "Design and finite element analysis of varying width piezoelectric cantilever beam to harvest energy." In *2015 International Conference on Energy, Power and Environment: Towards Sustainable Growth (ICEPE)*, pp. 1-6. IEEE, 2015.
[31] Sharpes, Nathan, Abdessattar Abdelkefi, and Shashank Priya. "Two-dimensional concentrated-stress low-frequency piezoelectric vibration energy harvesters." *Applied Physics Letters* 107, no. 9 (2015): 093901.
[32] Karami, M. Amin, and Daniel J. Inman. "Parametric study of zigzag microstructure for vibrational energy harvesting." *Journal of Microelectromechanical Systems* 21, no. 1 (2011): 145-160.

[33] Montazer, Babak, and Utpal Sarma. "Design and optimization of quadrilateral shaped PVDF cantilever for efficient conversion of energy from ambient vibration." *IEEE Sensors Journal* 18, no. 10 (2018): 3977-3988.

[34] Kim, Sunghwan, William W. Clark, and Qing-Ming Wang. "Piezoelectric energy harvesting with a clamped circular plate: analysis." *Journal of intelligent material systems and structures* 16, no. 10 (2005): 847-854.

[35] Shi, Qiongfeng, Tao Wang, Takeshi Kobayashi, and Chengkuo Lee. "Investigation of geometric design in piezoelectric microelectromechanical systems diaphragms for ultrasonic energy harvesting." *Applied Physics Letters* 108, no. 19 (2016): 193902.

[36] Wang, H. R., X. Xie, Y. T. Hu, and J. Wang. "Weakly nonlinear characteristics of a three-layer circular piezoelectric plate-like power harvester near resonance." *Journal of Mechanics* 30, no. 1 (2014): 97-102.]

[37] El-Hebeary, Mohamed MR, Mustafa H. Arafa, and Said M. Megahed. "Modeling and experimental verification of multi-modal vibration energy harvesting from plate structures." *Sensors and Actuators A: Physical* 193 (2013): 35-47.

[38] Dhote, Sharvari, Jean Zu, and Yang Zhu. "A nonlinear multi-mode wideband piezoelectric vibration-based energy harvester using compliant orthoplanar spring." *Applied Physics Letters* 106, no. 16 (2015): 163903.

[39] Hajati, Arman, and Sang-Gook Kim. "Ultra-wide bandwidth piezoelectric energy harvesting." *Applied Physics Letters* 99, no. 8 (2011): 083105.

[40] Masana, Ravindra, and Mohammed F. Daqaq. "Relative performance of a vibratory energy harvester in mono-and bi-stable potentials." *Journal of Sound and Vibration* 330, no. 24 (2011): 6036-6052.

[41] Stanton, Samuel C., Clark C. McGehee, and Brian P. Mann. "Nonlinear dynamics for broadband energy harvesting: Investigation of a bistable piezoelectric inertial generator." *Physica D: Nonlinear Phenomena* 239, no. 10 (2010): 640-653.

[42] Jung, Seok-Min, and Kwang-Seok Yun. "Energy-harvesting device with mechanical frequency-up conversion mechanism for increased power efficiency and wideband operation." *Applied Physics Letters* 96, no. 11 (2010): 111906.

[43] Fan, Kangqi, Jianwei Chang, Fengbo Chao, and Witold Pedrycz. "Design and development of a multipurpose piezoelectric energy harvester." *Energy Conversion and Management* 96 (2015): 430-439.

[44] Nguyen, Son, and Rajeevan Amirtharajah. "A hybrid RF and vibration energy harvester for wearable devices." In *2018 IEEE Applied Power Electronics Conference and Exposition (APEC)*, pp. 1060-1064. IEEE, 2018.

[45] Sang, Yingjun, Xueliang Huang, Hexiang Liu, and Ping Jin. "A vibration-based hybrid energy harvester for wireless sensor systems." *IEEE transactions on Magnetics* 48, no. 11 (2012): 4495-4498.

[46] Chen, Tao, Yuedong Xia, Wenjie Liu, Huicong Liu, Lining Sun, and Chengkuo Lee. "A hybrid flapping-blade wind energy harvester based on vortex shedding effect." *Journal of Microelectromechanical Systems* 25, no. 5 (2016): 845-847.

[47] Standards Committee of IEEE Ultrasonics. Ferroelectrics, and Frequency Control Society; IEEE Standard on Piezoelectricity: New York, NY, USA, 1987

[48] Dung, Cao Vu, and Eiichi Sasaki. "Numerical simulation of output response of PVDF sensor attached on a cantilever beam subjected to impact loading." *Sensors* 16, no. 5 (2016): 601.

[49] Beer, F.P.; Johnston, E.R.; Dewolf, J.T. Mechanics of materials, 5th ed.; McGraw-Hill Inc.: New York, NY, USA, 2006

[50] Erturk, Alper, and Daniel J. Inman. "A distributed parameter electromechanical model for cantilevered piezoelectric energy harvesters." *Journal of vibration and acoustics* 130, no. 4 (2008).

[51] Rammohan, S., C. Sanketh, C. M. Ramya, S. Jayanth Kumar, Jain Anjana, and Pratap Rudra. "Multi-layer piezoelectric energy harvesters for improved power generation." (2014): 1-6.

[52] Lu, F., H. P. Lee, and S. P. Lim. "Modeling and analysis of micro piezoelectric power generators for micro-electromechanical-systems applications." *Smart materials and structures* 13, no. 1 (2003): 57.

[53] Ambrosio, R., A. Jimenez, J. Mireles, M. Moreno, K. Monfil, and H. Heredia. "Study of piezoelectric energy harvesting system based on PZT." *Integrated Ferroelectrics* 126, no. 1 (2011): 77-86.

[54] Dechant, Eduard, Feodor Fedulov, Leonid Y. Fetisov, and Mikhail Shamonin. "Bandwidth widening of piezoelectric cantilever beam arrays by mass-tip tuning for low-frequency vibration energy harvesting." *Applied Sciences* 7, no. 12 (2017): 1324.

[55] Wang, Lu, Libo Zhao, Zhuangde Jiang, Guoxi Luo, Ping Yang, Xiangguang Han, Xiang Li, and Ryutaro Maeda. "High accuracy comsol simulation method of bimorph cantilever for piezoelectric vibration energy harvesting." *AIP Advances* 9, no. 9 (2019): 095067.

[56] Gilbert, James, Jing-Sheng Liu, Beng Lee Ooi, and Chung Ket Thein. "Modelling and optimisation of a bimorph piezoelectric cantilever beam in an energy harvesting application." *Journal of engineering science & technology* 11, no. 2 (2016).

[57] Trombetti, T., and S. Silvestri. "On the modal damping ratios of shear-type structures equipped with Rayleigh damping systems." *Journal of sound and vibration* 292, no. 1-2 (2006): 21-58.

[58] Kim, Miso, Mathias Hoegen, John Dugundji, and Brian L. Wardle. "Modeling and experimental verification of proof mass effects on vibration energy harvester performance." *Smart Materials and Structures* 19, no. 4 (2010): 045023.

[59] Liu, Huicong, Chengkuo Lee, Takeshi Kobayashi, Cho Jui Tay, and Chenggen Quan. "Investigation of a MEMS piezoelectric energy harvester system with a frequency-widened-bandwidth mechanism introduced by mechanical stoppers." *Smart Materials and Structures* 21, no. 3 (2012): 035005.

[60] Cho, Kyung-Hoon, Hwi-Yeol Park, Jin S. Heo, and Shashank Priya. "Structure–performance relationships for cantilever-type piezoelectric energy harvesters." *Journal of Applied Physics* 115, no. 20 (2014): 204108.

[61] Gu, Lei. "Low-frequency piezoelectric energy harvesting prototype suitable for the MEMS implementation." *Microelectronics Journal* 42, no. 2 (2011): 277-282.

[62] Arroyo, Emmanuelle, Adrien Badel, Fabien Formosa, Yipeng Wu, and J. Qiu. "Comparison of electromagnetic and piezoelectric vibration energy harvesters: Model and experiments." *Sensors and Actuators A: Physical* 183 (2012): 148-156.

[63] Kanno, I., K. Sagawa, R. Oka, H. Kotera, J. Ogawa, N. Yamauchi, K. Aizawa, and T. Matsushima. "Piezoelectric energy harvesters of PZT films deposited on titanium cantilevers." *Power MEMS* 10 (2010): 379-382.

[64] Wang, Q., Z. P. Cao, and H. Kuwano. "Metal-based piezoelectric energy harvesters by direct deposition of PZT thick films on stainless steel." *Micro & Nano Letters* 7, no. 12 (2012): 1158-1161.

[65] Tang, G., J-Q. Liu, B. Yang, J-B. Luo, H-S. Liu, Y-G. Li, C-S. Yang, V-D. Dao, K. Tanaka, and S. Sugiyama. "Piezoelectric MEMS low-level vibration energy harvester with PMN-PT single crystal cantilever." *Electronics letters* 48, no. 13 (2012): 784-786.

[66] Sun, Chengliang, Lifeng Qin, Fang Li, and Qing-Ming Wang. "Piezoelectric energy harvesting using single crystal Pb (Mg1/3Nb2/3) O 3-xPbTiO3 (PMN-PT) device." *Journal of Intelligent Material Systems and Structures* 20, no. 5 (2009): 559-568.

[67] Won, Sung Sik, Joonhee Lee, Vineeth Venugopal, Dong-Joo Kim, Jinkee Lee, Ill Won Kim, Angus I. Kingon, and Seung-Hyun Kim. "Lead-free Mn-doped (K0. 5, Na0. 5) NbO3 piezoelectric thin films for MEMS-based vibrational energy harvester applications." *Applied Physics Letters* 108, no. 23 (2016): 232908.

[68] Cao, Ziping, Jinya Zhang, and Hiroki Kuwano. "Design and characterization of miniature piezoelectric generators with low resonant frequency." *Sensors and Actuators A: Physical* 179 (2012): 178-184.

[69] Takise, Hiroki, Tomokazu Takahashi, Masato Suzuki, and Seiji Aoyagi. "Fabrication of piezoelectric vibration energy harvester using coatable PolyVinylidene DiFluoride and its characterisation." *Micro & Nano Letters* 12, no. 8 (2017): 569-574.

[70] Song, Jundong, Guanxing Zhao, Bo Li, and Jin Wang. "Design optimization of PVDF-based piezoelectric energy harvesters." *Heliyon* 3, no. 9 (2017).

[71] Jiang, Yonggang, Syohei Shiono, Hiroyuki Hamada, Takayuki Fujita, Kohei Higuchi, and Kazusuke Maenaka. "Low-frequency energy harvesting using a laminated PVDF cantilever with a magnetic mass." *Power MEMS* 375378 (2010).

[72] Cao, Ziping, Jinya Zhang, and Hiroki Kuwano. "Vibration energy harvesting characterization of 1 cm2 Poly (vinylidene fluoride) generators in vacuum." *Japanese Journal of Applied Physics* 50, no. 9S2 (2011): 09ND15.

[73] Rammohan, S., C. M. Ramya, S. Jayanth Kumar, Anjana Jain, and Rudra Pratap. "Low frequency vibration energy harvesting using arrays of PVDF piezoelectric bimorphs." *J. Inst. Smart Struct. Syst.* 3, no. 1 (2014): 18-27.

[74] Finot, Eric, Ali Passian, and Thomas Thundat. "Measurement of mechanical properties of cantilever shaped materials." *Sensors* 8, no. 5 (2008): 3497-3541.

[75] Jianqiang, Han, Zhu Changchun, Liu Junhua, and He Yongning. "Dependence of the resonance frequency of thermally excited microcantilever resonators on temperature." *Sensors and Actuators A: Physical* 101, no. 1-2 (2002): 37-41.

[76] Malzbender, Jürgen. "Mechanical and thermal stresses in multilayered materials." *Journal of applied physics* 95, no. 4 (2004): 1780-1782.

[77] "Temperature humidity chamber," Guangdong Yuanyao Test Equipment Co., Ltd [interactive][last accessed on 2019-08-24] available at http//http//www.gdmypt.com/.

[78] Ito, Y. "Piezoelectricity Wiley Encyclopedia of Electrical and Electronics Engineering ed J Webster." (1999).

[79] Erturk, Alper. "Electromechanical modeling of piezoelectric energy harvesters." PhD diss., Virginia Tech, 2009.

[80] Wang, J-J., C-E. Lu, S-C. Lo, Y-C. Su, and W. Fang. "Composite rubber electret for electromechanical load detection." In *2017 19th International Conference on Solid-State Sensors, Actuators and Microsystems (TRANSDUCERS)*, pp. 1368-1371. IEEE, 2017.